Journal of Medicinal Chemistry Article

J. Med. Chem. **2009,** *52,* 4725–4742 **4725**
DOI: 10.1021/jm9002654

Magnetic Resonance Molecular Imaging of Vascular Cell Adhesion Molecule-1 Expression in Inflammatory Lesions Using a Peptide-Vectorized Paramagnetic Imaging Probe

Carmen Burtea,[†] Sophie Laurent,[†] Marc Port,[‡] Eric Lancelot,[‡] Sébastien Ballet,[‡] Olivier Rousseaux,[‡] Gérard Toubeau,[§] Luce Vander Elst,[†] Claire Corot,[‡] and Robert N. Muller*[,†]

[†]*Department of General, Organic and Biomedical Chemistry, NMR and Molecular Imaging Laboratory, University of Mons, 24 Avenue du Champ de Mars, B-7000 Mons, Belgium,* [‡]*Guerbet, Research Center, 16-24 Rue Jean Chaptal, 93600 Aulnay-sous-Bois, France, and* [§]*Laboratory of Histology, University of Mons, Pentagon 1B, 6 Avenue du Champ de Mars, B-7000 Mons, Belgium*

Received March 2, 2009

The vascular cell adhesion molecule-1 (VCAM-1) has distinct roles in inflammatory cell recruitment to the damaged vessel wall. In the present work, a cyclic heptapeptide phage displayed library was screened in vitro during four rounds of biopanning. On the basis of K_d and IC_{50} values, a peptide (encoded as R832) was selected for in vitro and in vivo validation. After conjugation to Gd-DOTA, VCAM-1 imaging was assessed by MRI on a model of T cell mediated hepatitis, induced in mice by concanavalin A. On histological samples, the location of biotinylated R832 (R832-Bt) around liver veins in hepatitis resembles the pattern of MRI enhancement. Gd-DOTA-R832 was then assessed on $ApoE^{-/-}$ mice and produced an important signal enhancement of the aortic wall, while R832-Bt interacted with morphologic structures comparable to those marked by anti-VCAM-1 antibody. In conclusion, the in vitro and in vivo evaluation of peptide R832 suggests a specific interaction with the targeted biomolecule. Its conjugation to imaging reporters could assist the diagnosis of inflammatory diseases.

1. Introduction

Inflammation is a dynamic process involving activation of multiple signaling pathways governing the recruitment of various leukocytes to different sites of inflammation. This process engages leukocyte rolling on the vascular endothelium, followed by activation, adhesion, and transmigration into inflamed tissue. The cell adhesion molecules (CAMs[a]) have distinct roles in inflammatory cell recruitment to the activated vascular endothelium. Among them, the vascular cell adhesion molecule-1 (VCAM-1) is an immunoglobulin-like CAM that binds to very late antigen-4 (VLA-4, $\alpha_4\beta_1$) integrin, which is constitutively expressed on lymphocytes, monocytes, and eosinophils. Depending on the avidity status of VLA-4 integrin, VCAM-1 mediates both rolling-type adhesion and firm adhesion. As opposed to other immunoglobulin-like CAMs, VCAM-1 is not expressed under baseline conditions but is rapidly induced in activated vascular endothelium. The expression of CAMs is primarily regulated by NF-κB and AP-1 transcription factors, which are in turn activated by proinflammatory cytokines (i.e., IL-1β, TNF-α).[1,2]

Atherosclerosis, a progressive disease characterized by the deposition of lipids and fibrous elements in the wall of large arteries, contributes to the development of cardiovascular disease. Atherosclerosis develops in response to vascular injury and involves inflammation and vessel remodeling. The recruitment of inflammatory cells in atherosclerotic lesions is a constitutive phenomenon throughout the process of lesion initiation and plaque growth. VCAM-1 is up-regulated under inflammatory conditions in both precocious and vulnerable atherosclerotic lesions, where it binds to monocytes and T lymphocytes. Vascular injury is induced by multiple insults including hypercholesterolemia, diabetes, smoking, and hypertension. VCAM-1 is expressed by endothelial cells (ECs) in response to cholesterol feeding selectively in areas prone to lesion formation.[3−5] Constituents of modified lipoprotein particles, such as oxidized phospholipids and short-chain aldehydes, can induce transcriptional activation of the VCAM-1 gene mediated in part by NF-κB.[6,7] A selective expression of VCAM-1 has also been observed at branch points of arteries, which are exposed to disturbed rather than to laminar flow. Several genes with "atheroprotective" properties (i.e., superoxide dismutase and NO-synthase) contain shear-stress response elements in their promoter regions that may modulate NF-κB activation, limiting thus VCAM-1 expression and other inflammatory pathways.[8,9]

In atherosclerotic plaques, VCAM-1 is moreover expressed by ECs of the microvascular network of vasa vasorum. Neovascularisation and expression of CAMs by microvessels at sites of vulnerable lipid-rich plaques could contribute to plaque destabilization.[10,11] The smooth muscle cells (SMCs) in injured arteries also express VCAM-1 after their conversion

*To whom correspondence should be addressed. Phone/Fax: +32-65373520. E-mail: Robert.Muller@umons.ac.be.

[a] Abbreviations: VCAM-1, vascular cell adhesion molecule-1; MRI, magnetic resonance imaging; R832-Bt, biotinylated R832; CAMs, cell adhesion molecules; ECs, endothelial cells; SMCs, smooth muscle cells; MCP-1, monocyte chemoattractant protein-1; HUVEC, human umbilical vein endothelial cells; AI, affinity index; CAs, contrast agents; Gd-DOTA, 1,4,7,10-tetraazacyclododecane-1,4,7,10-tetraacetic acid; ConA, concanavalin A; ABTS, [2,2′-azino-bis(3-ethylbenzthiazoline-6-sulfonic acid)]; SI, signal intensity; MSME, multislice−multiecho; RARE, rapid acquisition with relaxation enhancement; TOF, time-of-flight; DAB, 3,3′-diaminobenzidine; NMRD, nuclear magnetic relaxation dispersion.

Published on Web 07/06/2009

from a contractile phenotype to an activated secretory state. VCAM-1 is coexpressed with monocyte chemoattractant protein-1 (MCP-1) and promotes infiltration of macrophages into the vessel wall. VCAM-1 and intercellular CAM 1 (ICAM-1) expression leads to enhanced adhesion of α_4-integrin-positive lymphocytes and β_2-integrin-expressing monocytes.[12,13]

It is now well accepted that sudden cardiovascular events are not always preceded by particular symptoms and often result from plaque rupture at sites with no or only modest stenosis (i.e., luminal narrowing) at angiography.[14] Hence, there is a considerable demand for diagnostic procedures that specifically identify rupture-prone, vulnerable plaques as the most frequent cause of sudden cardiac events.[15] The CAMs expressed by plaque components are rigorously regulated during the pathogenesis of atheroma and may be associated with a certain stage of it. This makes them appropriate targets for the next generation of diagnosis and therapeutic molecules because their detection and/or modulation could help evaluating the stage of atherosclerotic disease and may assist its treatment accordingly, which is the basis of a theranostic approach.

In the case of diagnosis, molecularly targeted imaging probes have gained great popularity during the past decade[16,17] in the context of theranostic strategies. The imaging of VCAM-1 expression has thus been approached with antibodies or peptides conjugated to nuclear,[18] magnetooptical,[19,20] or ultrasound probes.[21] However, the size of most atherosclerotic lesions is below the spatial resolution of nuclear or ultrasound imaging systems. To overcome this limitation, an important target-to-background ratio is required, which could be attained only with highly specific targeting molecules. Nuclear medicine has the advantage of a superior sensitivity against low probe concentrations, but the targeted molecule could be roughly associated with a certain anatomic structure, in particular that related to the artery wall. In addition to the low anatomic resolution at larger penetration depths characterizing ultrasound imaging systems, the large size of ultrasound probes renders them less accessible to the targeted sites. The only clinical imaging technique able to attain a spatial resolution in the order of micrometers is magnetic resonance imaging (MRI), but this is often obtained at high magnetic fields (> 3 T, with the clinical magnetic field regularly being at 1.5 T), with long acquisition times (> 1 h), and by using especially adapted surface or intravascular coils. The low sensitivity achieved with magnetic probes constitutes a supplementary challenge for molecular targeting by MRI. Owing to their large NMR efficacy (i.e., relaxivity), iron oxide nanoparticles may represent an attractive probe alternative.[22] However, the negative contrast, the restrained diffusion through biologic pores, and inefficient stealth even after pegylation make them less robust for certain in vivo applications where the endogenous signal hypointensity or the inaccessible location of the targeted biomolecule may be at the origin of a poor image contrast. Nevertheless, these agents were reported to be successful in molecular imaging of various experimental models, such as the acute inflammation of the mouse brain (VCAM-1 targeting with antibody conjugated microparticles),[23] the ex vivo imaging of atherosclerotic aorta of ApoE$^{-/-}$ mice (VCAM-1 and P-selectin targeting with antibody-conjugated microparticles),[24] the brains of malaria-infected mice (targeting of activated glycoprotein IIb/IIIa receptors with antibody conjugated microparticles),[25] and the ex vivo imaging of human carotid plaques (targeting of activated glycoprotein IIb/IIIa receptors with antibody conjugated microparticles).[26] Interesting clinical applications of nonfunctionalized iron oxide particulate agents were reported, for instance, in the imaging of the malignant brain tumors[27] or of the pancreatic islet grafts in diabetic patients.[28] In addition to this, several techniques have been developed lately to convert the negative contrast into a positive one either by using dedicated MR sequences[29] or by employing a postprocessing method that is applied to the acquired image data.[30]

The robust noninvasive molecular imaging of atherosclerotic plaque biology depends, however, on the detection threshold of the imaging system, on the target/background signal, and on the molecular targeting reproducibility. On the basis of the current clinical demands for plaque imaging, the aim of the present work was to develop a VCAM-1-targeted low molecular weight magnetic probe by using a cyclic heptapeptide ligand identified by phage display technology. Various low molecular weight paramagnetic probes were previously described in literature for molecular imaging of E-selectin in inflammatory pathologies[31,32] and of the $\alpha_v\beta_3$ integrin expression in atherosclerotic plaque.[11] VCAM-1 targeting with specific contrast agents (CAs) is interesting for several reasons: (1) VCAM-1 is a biomarker of early atherosclerotic lesions and of mature vulnerable plaques, which could be distinguished on MR images because of the micrometer anatomical resolution; (2) this CAM is easily accessed by CAs through the microvessels present in lipid-rich plaques; and (3) the molecule may have a therapeutic effect by inhibiting the leukocytes' adhesion to endothelium. It is moreover worthy to mention that peptides provide now valuable alternatives to various biopharmaceuticals, such as the antibodies. Peptides bind various targets with high affinity and specificity, and many medicines marketed today are from this class of small molecule agents.[33] The peptides or other small molecule ligands are intended to solve the shortcomings of their protein counterparts (e.g., antibodies or natural ligands of biomolecules), such as the cost of production, the protein antigenicity, and the restrained diffusion to the targeted sites due to their larger size.

2. Results

2.1. Characterization of the Candidate Phage Clones. 2.1.1. Affinity for VCAM-1 of the Candidate Phage Clones. After four rounds of panning, 42 phage clones were isolated and their affinity was evaluated both on mouse and human recombinant VCAM-1 and on human umbilical vein endothelial cells (HUVEC) expressing the VCAM-1 by stimulation with TNFα (HUVEC/TNFα). In the case of HUVEC, various competition experiments were carried out aiming, on the one hand, to confirm the specific interaction of the peptide ligands with VCAM-1 and, on the other hand, to validate their potential to inhibit the adhesion to VCAM-1 of VLA-4 expressing cells. The competition tests involved hence either the receptor sites (VCAM-1 in solution or expressed by HUVEC) or the natural ligand of VCAM-1 (VLA-4 integrin) expressed by Jurkat T lymphocytes (blocking of the cell adhesion).

Three competition experiments were performed: (1) preincubation of phages with VCAM-1 in solution, followed by their incubation with HUVEC; (2) preincubation of phages with HUVEC, followed by the addition of Jurkat cells; and (3) preincubation of Jurkat cells with HUVEC, followed by

the addition of phages. The binding of phages to TNF-α-stimulated HUVEC or control cells was also evaluated.

With the aim to express in one single term the affinity for VCAM-1 reflected by various tests of validation, we have conceived the term of "affinity index" (AI), which is defined by the following equation:

$$\mathrm{AI} = \left[\frac{\left(\frac{\mathrm{hVCAM1}\times\mathrm{mVCAM1}\times\mathrm{HUVEC}}{\mathrm{hVCAM1_{pre}}}\right)^2}{\sqrt{(\mathrm{Jurkat_{post}}\times\mathrm{Jurkat_{pre}})}}\right]\times 100$$

where hVCAM1 = affinity for human recombinant VCAM-1 expressed by OD_{405}, mVCAM1 = affinity for mouse recombinant VCAM-1 expressed by OD_{405}, HUVEC = affinity for HUVEC/TNFα expressed by OD_{405}, $hVCAM1_{pre}$ = % binding inhibited by preincubation with human VCAM-1 in solution (normalized to OD_{405} of HUVEC/TNFα), $Jurkat_{post}$ = % binding inhibited by postincubation with Jurkat cells (normalized to OD_{405} of HUVEC/TNFα), $Jurkat_{pre}$ = % binding inhibited by preincubation with Jurkat cells (normalized to OD_{405} of HUVEC/TNFα)

The results obtained with this coefficient are represented in Figure 1A, which highlights the phage clones 10, 22, 40, and 41 as presenting an optimal binding to the target. For clarity, the results obtained with these phage clones during various affinity tests are presented in Figure 1B and Figure 1C. Their affinity for human and mouse VCAM-1 is comparable (Figure 1B), while that for HUVEC/TNFα is generally higher than that for nonstimulated cells (107−189%) (Figure 1C). The immunodetection of VCAM-1 expressed by HUVEC has evidenced an OD_{405} of 0.452 ± 0.072 for the cells stimulated with TNFα and of 0.278 ± 0.039 for nonstimulated cells. These values show 162% higher VCAM-1 expression by stimulated HUVEC and indicate a certain baseline level of expression by resting cells. Our results corroborate the data reported in the specialized literature[34,35] and can be compared to the binding level of the phage clone 40, which shows 189% higher interaction with HUVEC/TNFα over control cells. Various competition experiments (Figure 1C) attested to a specific target binding, particularly in the case of clone 40 which was significantly inhibited by VCAM-1 in solution (63% binding normalized to OD_{405} of HUVEC/TNFα) and by the preincubation with Jurkat cells (31% binding normalized to OD_{405} of HUVEC/TNFα); the postincubation with Jurkat cells did not dislocate phages from the binding sites.

2.1.2. Peptide Sequence of the Selected VCAM-1 Ligands after Four Rounds of Panning. The DNA of the phage clones isolated after three and four rounds of panning was sequenced, and their peptide structure was deciphered (Figure 2). The consensus motifs are presented in Figure 2A; all the sequences are flanked by Cys, but this amino acid is not shown in order to better distinguish the consensus motifs.

The sequences presenting the amino acids Thr, Arg, and Leu seem to be enriched after four rounds of panning. Three sequences (WSRTLTA, NNSKSHT, and EGGRMKY) were rescued equally after the third and the fourth round of panning.

The percentage frequency of amino acids in the peptide sequence (Figure 2B) emphasizes those that may have relevance for VCAM-1 interaction. The amino acids Arg, Leu, Ser, and Thr are the most frequent (they surpass the level of mean + variance) in the peptide structure, while Gly, Pro, and His are quite well represented (they surpass the mean).

2.1.3. Peptide Sequence of the Phage Clones Presenting an Optimal Affinity for VCAM-1. The sequence of the four phage clones (10, 22, 40, and 41) presenting an optimal affinity for VCAM-1 is presented in Table 1. The amino acids Thr, Arg, and Leu are almost constantly represented in each sequence, which could signify that they are essential for this interaction. Although not always in a close position to the RTL/TRL motif, the amino acid Ser is also present in two peptides; when present, the amino acid Asp is located in the vicinity of RTL/TRL. The peptide alignment with adhesion molecules (integrin, protocadherin) or with immunoglobulin receptors shows that peptide selection is not accidental.

2.2. Characterization of the Candidate VCAM-1-Specific Peptide Ligands. The results of the previous tests of affinity indicate that peptides C-RTTSDAL-C (clone 10), C-HLGARTH-C (clone 22), C-NNSKSHT-C (clone 40), and C-MKTDTRL-C (clone 41) have an optimal affinity for VCAM-1. These peptides were selected for subsequent in vitro and eventually in vivo evaluation after their synthesis. For convenience, the peptides were encoded as follows: clone 41 = R831, clone 40 = R832, clone 22 = R833, and clone 10 = R834.

2.2.1. K_d and IC_{50} of the Selected Peptides. The K_d of VCAM-1-binding peptides ranges from 1.03×10^{-5} M to 9.14×10^{-5} M (Table 2). The peptide presenting the most important affinity for VCAM-1 is that corresponding to the phage clone 40 (peptide R832).

The IC_{50} was evaluated by a competition experiment with Jurkat cells (Table 2). This parameter ranged from 6.3×10^{-5} M to 57×10^{-5} M, with peptide R832 presenting the most important potential to inhibit cell adhesion. As a positive control, the IC_{50} value of anti-VCAM-1 antibody estimated in the same experimental conditions was 1.35×10^{-6} M.

2.2.2. In Vivo MRI Evaluation of Gd-DOTA-R832. On the basis of its affinity constants, peptide R832 was selected for in vivo evaluation by MRI on animal models of inflammation characterized by VCAM-1 expression. The peptides were conjugated to gadolinium 1,4,7,10-tetraazacyclododecane-1,4,7,10-tetraacetate (Gd-DOTA) using squarate group as a linker. This group allows the easy grafting of the peptide on Gd-aminobutyl-DOTA via the N-terminal function and has already been used successfully for the synthesis of MRI CAs.[36] After conjugation, peptide R832 (Gd-DOTA-R832) and its scramble (HSCNKNSCT) homologue (Gd-DOTA-R832.sc) were assessed by MRI on a well documented model of T cell mediated hepatitis induced in mice by concanavalin A (ConA) and on the $ApoE^{-/-}$ mouse model of atherosclerosis.

2.2.2.1. Physicochemical Characterization of the Contrast Agents. The NMRD profiles of R832/R832.sc derivatives and of the parent compound Gd-DOTA are given in Figure 3A. The proton NMRD profiles were fitted using a theoretical model described earlier.[37] Parameters obtained by the fitting are summarized in Figure 3A (fixed parameters: $q = 1$, $d = 0.31$ nm, $D = 3.3\ 10^{-9}$ m^2/s, $\tau_M = 100$ ns). Compared to the NMRD profile of the parent compound Gd−DOTA, the observed relaxivity of the new complexes is markedly larger. The stability of the new complexes was tested by measuring the exchange between the gadolinium and the zinc ions (Figure 3B). Gd-DOTA-R832 and Gd-DOTA-R832.sc have shown a very good stability versus zinc transmetalation (evaluated as described in ref 38) with decomplexation less than 5% after 5000 min.

2.2.2.2. VCAM-1 Targeting in ConA Hepatitis. (A) VCAM-1 Expression in ConA Hepatitis and Its Colocalization with R832

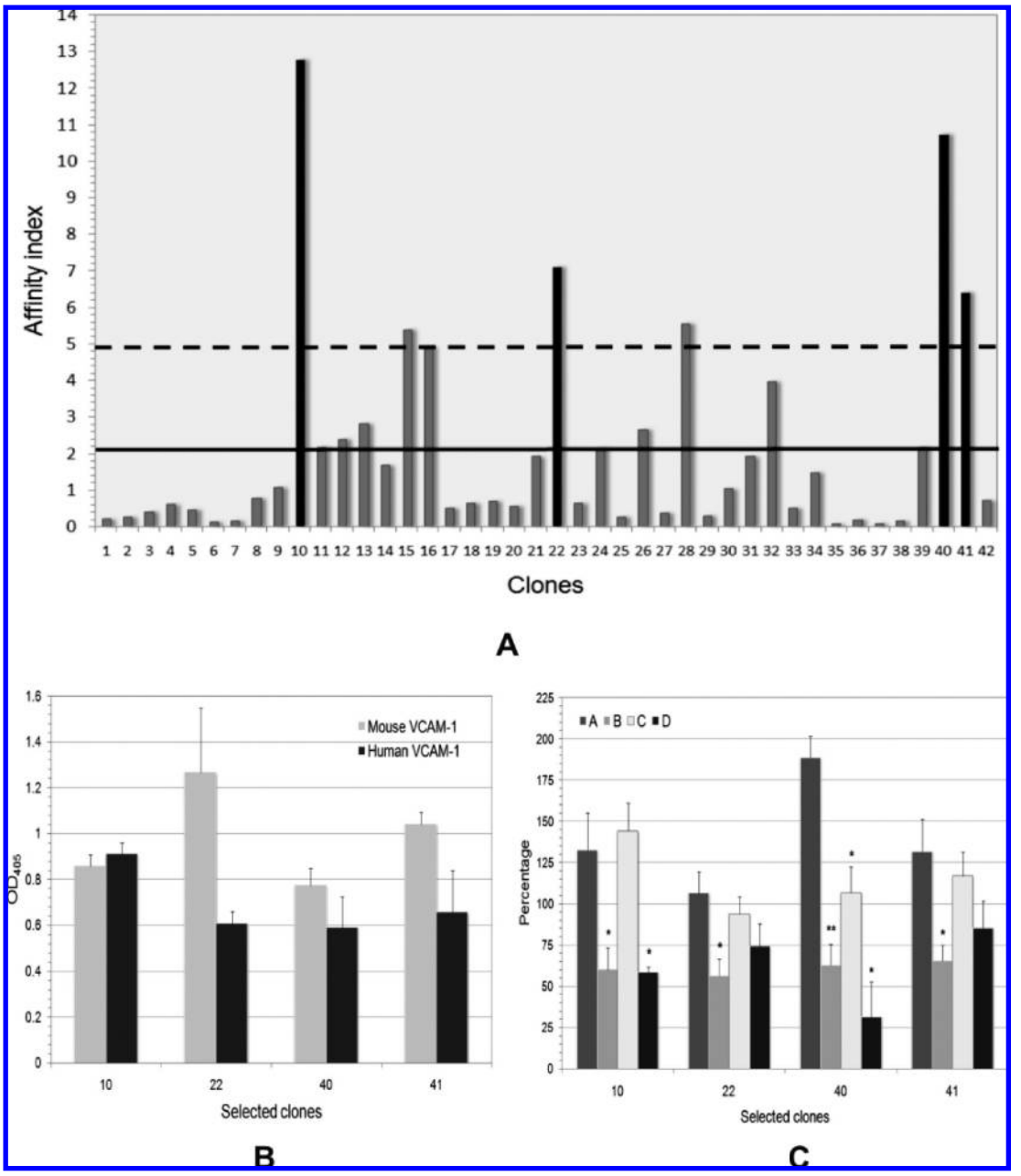

Figure 1. Screening of the affinity for VCAM-1 of the phage clones isolated after four rounds of panning. (A) Affinity index (AI) describing the interaction with VCAM-1. The solid line represents the mean, and the dotted line represents the mean + variance. (B) Comparative affinity for mouse and human recombinant VCAM-1 of the selected phage clones. (C) Percentage of interaction at the receptor sites (VCAM-1 expressed by HUVEC) of the selected phage clones in various competition experiments (the percentage of binding is normalized to OD_{405} of HUVEC/TNFα): A = % HUVEC + TNFα/HUVEC; B = % binding inhibited by preincubation with human VCAM-1 in solution; C = % binding inhibited by postincubation with Jurkat cells; D = % binding inhibited by preincubation with Jurkat cells. The results are represented as the mean ± SEM ($n = 3$). Statistical significance was calculated by Student t test: for part C, $* = p < 0.05$, $** = p < 0.01$ by comparison to part A.

Binding. Biotinylated R832 (R832-Bt) immunostained the hepatic tissue around the liver veins of ConA mice (Figure 4A,B) and colocalized with VCAM-1 expression as confirmed with a specific antibody (Figure 4E,F). No significant R832 binding and VCAM-1 expression was observed in healthy liver tissue (Figure 4C,G). The secondary antibodies were not responsible for the particular immunostaining produced by R832-Bt and anti-VCAM-1 antibody as confirmed by the negative control samples (Figure 4D,H).

(B) MR Imaging of VCAM-1 Expression. The MR images obtained with Gd-DOTA-R832 and the nonspecific CA Gd-DOTA are presented in Figure 5. Both CAs were evaluated on mice with ConA-induced hepatitis and on healthy mice.

An individual variability of the kinetics of signal enhancement was observed with Gd-DOTA-R832 in pathological conditions, which was probably related to the timing of VCAM-1 expression. An example of MR imaging of VCAM-1 expression with Gd-DOTA-R832 is shown in parts A1−A4 of Figure 5, where hepatic vasculature is progressively enhanced attaining its maximum level 92 min postcontrast (~6.5 h after ConA injection). Such an enhancement of liver veins was not observed either in healthy mice injected with VCAM-1-targeted CA (Figure 5B) or in mice with ConA

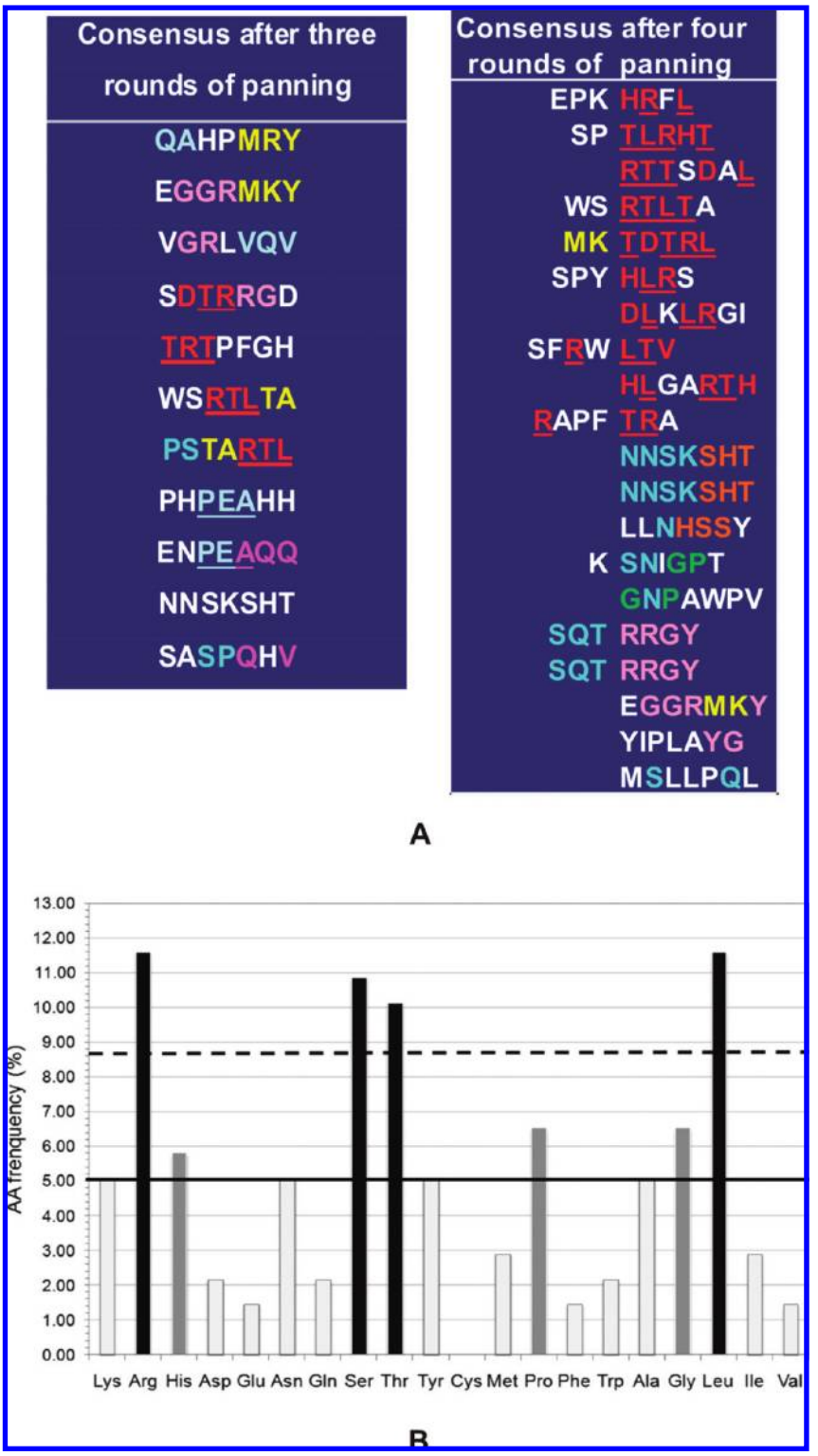

Figure 2. Amino acid composition of the phage clones isolated after three and four rounds of panning: (A) consensus amino acid motifs after four rounds of panning as compared to the third round of panning; (B) amino acid frequency in peptide structure. Solid line represents the mean; dotted line represents the mean + variance.

hepatitis injected with Gd-DOTA (Figure 5C). Gd-DOTA-R832 was excreted by renal route (data not shown); no biliary elimination could be detected.

The signal intensity (SI) enhancement (ΔSNR%) produced in liver by Gd-DOTA-R832 and Gd-DOTA is presented in Figure 5D. In livers with hepatitis, the VCAM-1-targeted CA enhanced the SI at the highest level among the four experimental groups. The ΔSNR% increased to 60−65% during the first 15 min postcontrast. It decreased to ∼55% until ∼1 h postcontrast, while subsequently the signal evolution was variable.

The ΔSNR% in the three other experimental groups was lower and similar, with a maximum SI of 39−47% during the first 7 min postcontrast; the SI progressively decreased until the end of the MRI session.

Table 1. Peptide Sequences of the Four Selected Phage Clones[a]

clone (peptide)	peptide alignment
10 (C-**RTTSDAL**-C)	low affinity IgE Fc receptor (RTASDSL) (AN: P20693) Fc ε receptor II (RTASDSL) (AN: Q8 VH33)
22 (C-H**L**GA**RT**H-C)	leukocyte IgG-like receptor subfamily (LGPRTH) (AN: A6NI73)
40 (C-NN**S**K**S**H**T**-C)	leukocyte Ig-like receptor B (NSQSHT) (AN: Q8MJZ5) leukocyte common antigen-related protein (NSKAHT) (AN: Q9QW67) protocadherin (NHSKSH) (AN: Q9WU10)
41 (C-MK**T**D**TRL**-C)	integrin α-2b (MKKDTRI) (AN: Q9QUM0) integrin α-4 precursor (KTDKRL) (AN: P13612)

[a] Alignment with relevant protein sequences (identified with Swiss-Prot accession numbers, AN) is also shown. The frequent motifs (bold) and amino acids (bold underlined) are highlighted.

Table 2. K_d Values of the Four Heptapeptides for the Interaction with VCAM-1 and Their IC_{50} Values Estimated in Competition with Jurkat Cells

peptide	K_d (M)	IC_{50} (M)
R831	4.26×10^{-5}	8.7×10^{-5}
R832	1.03×10^{-5}	6.3×10^{-5}
R833	9.14×10^{-5}	8.3×10^{-5}
R834	8.94×10^{-5}	57×10^{-5}

2.2.2.3. VCAM-1 Targeting in ApoE$^{-/-}$ Mice. (A) VCAM-1 Expression in Aorta of ApoE$^{-/-}$ Mice and Its Colocalization with R832-Bt Binding. Histological sections of the abdominal aorta harvested from ApoE$^{-/-}$ mice confirmed the presence of atherosclerotic lesions (Figure 6) characterized by extensive expression of VCAM-1 both in intima (Figure 6A) and in media layers (Figure 6B), where possible angiogenic neovessels can be distinguished. VCAM-1 expression (Figure 6C) colocalized with R832-Bt immunostaining (Figure 6D) on histological sections located in the same area of the abdominal aorta.

(B) MR Imaging of VCAM-1 Expression. The images of atherosclerotic plaque obtained on ApoE$^{-/-}$mice with Gd-DOTA-R832 are presented in Figure 7. The plaque is mainly enhanced around the aortic lumen, probably corresponding to higher VCAM-1 expression in the endothelial layer. The plaque enhancement produced by the nonspecific CA Gd-DOTA did not allow the optimal discrimination of the atheroma from the surrounding tissues (Figure 7A). The images acquired with the TOF protocol (Figure 7B) evidence a particularly bright contour around the aortic lumen, which corresponds to the localization of signal enhancement in the RARE protocol. An interesting plaque enhancement produced in the renal artery by Gd-DOTA-R832 is shown in Figure 7C, where Gd-DOTA-R832.sc could not produce a comparable effect.

The ΔSNR% measured on RARE images (Figure 7D) confirms that Gd-DOTA-R832 was able to generate an important signal enhancement of the aortic wall, although this was quite variable among the investigated animals and regions of the aorta as indicated by the SEM values. The signal attained a maximum at 10 min (111%) postcontrast and was constantly high until 58 min (87%), when the imaging session was finished. In the case of Gd-DOTA-R832.sc, the ΔSNR% ranged between 73% and 51%, while Gd-DOTA produced a signal enhancement of 71−28%.

The preinjection of peptide R832 ∼15 min prior to Gd-DOTA-R832 (Figure 8A) attenuated the positive contrast produced by this last one, suggesting thus that both the peptide and the vectorized contrast agent interact with the same target in atherosclerotic plaque. The ΔSNR% (Figure 8B) reached its minimum level (45%) at 42 min postcontrast, while the enhancement produced by Gd-DOTA-R832 in the absence of the competitor was twice as much (92%) at the same time point.

In control C57BL/6J mice, neither Gd-DOTA-R832 (Figure 9A) nor Gd-DOTA-R832.sc (Figure 9B) produced any particular enhancement of the aortic wall.

3. Discussion and Conclusions

VCAM-1 is an important biomarker of various inflammatory disorders having a particular relevance for the pathological process of atherosclerotic disease. Phage display was used in the present work to detect peptide binders with specific affinity for VCAM-1, which would be highly relevant for the diagnosis of early atherosclerotic lesions and of mature vulnerable plaques.

After three rounds of panning, a certain consensus has been found for several peptide motifs, such as RTL and GR, amino acids that were enriched in the peptides rescued after four rounds of panning together with S, G, P, and H. The amino acids R, S, T, and H are polar, are either ionizable (R and H) or not (S and T), and can contribute to ion coordinating during interaction with VCAM-1 (T and S) or can contract an ionic or hydrogen binding with the key residues on domain II of VCAM-1 (LEDADRKSL).[39] The amino acids L and G may stabilize the interaction with VCAM-1 by a hydrophobic binding. When present, D is situated in the vicinity of TRL. The peptide sequence NNSKSHT (clone 40) is quite different from the others, but the amino acids in its structure are a reminder of the active site of VLA-4 integrin. According to the models of VCAM-1/VLA-4 interaction,[39] T206 is a metal ion coordinating residue in the β1 subunit of VLA-4 located close to N207 and K208; L205 and P228 in the same subunit share close hydrophobic interaction with VCAM-1, while Y and G are essential for the binding of the VLA-4 α4 subunit to VCAM-1 (its mutation completely blocks the binding to VCAM-1). In addition, D is part of the putative divalent cation site of the integrin α4 subunit[40,41] and is a key binding residue in the β1 subunit, while K is important for the β1 binding selectivity compared to β7 integrin.[39] Each of the three putative divalent cation sites of the integrin α4 subunit has the amino acid sequence D-X-D(or N)-X-D(or N)-G-XX-D, which partly resembles the EF-hand motif of Ca^{2+}-binding proteins, such as calmodulin and troponin C. Although without a clearly defined function in ligand binding, the sequence LLRTR is also present in the seventh repeat (residues 390−432), β-strand 3, of the integrin α-4 subunit.[40]

The peptide alignment with adhesion molecules (integrin, protocadherin) or with immunoglobulin receptors shows that peptide selection was not accidental.

The four selected phage clones presented an important affinity for both mouse and human VCAM-1, and they were able to inhibit cell adhesion. Among them, phage clone

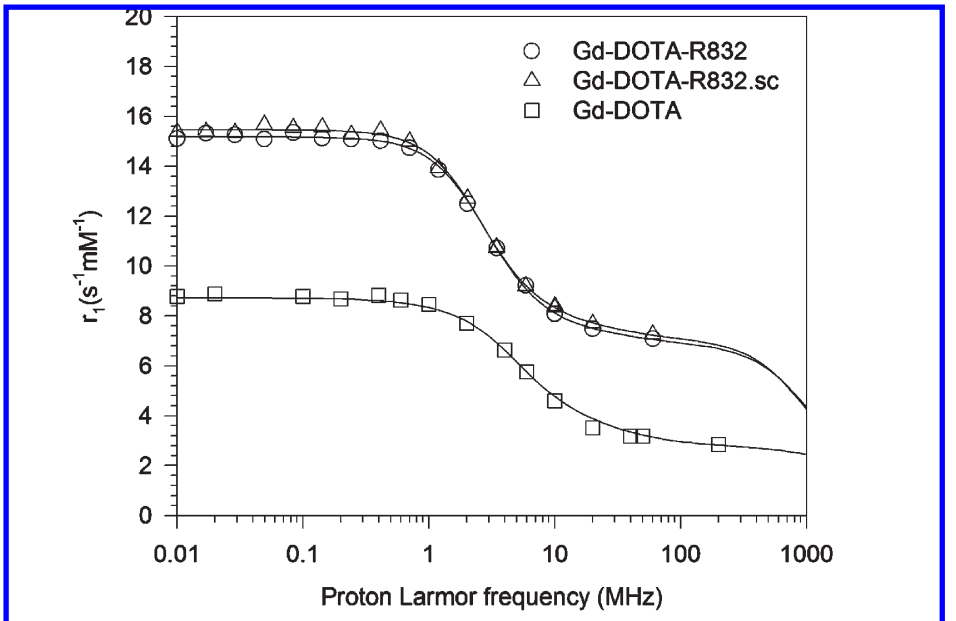

Complexes	τ_R (ps)	τ_M (ns)	τ_{SO} (ps)	τ_V (ps)	τ_{SS} (ps)	q_{SS}
Gd-DOTA-R832	153±5.3	100	236±16.5	22.4±2.7	38.8±6.4	1.77±0.05
Gd-DOTA-R832sc	162±4.9	100	248±18.3	24.4±3.7	34.7±3.8	1.76±0.09
Gd-DOTA[Ref38]	53±1.3	122±10	404±24	7±1		

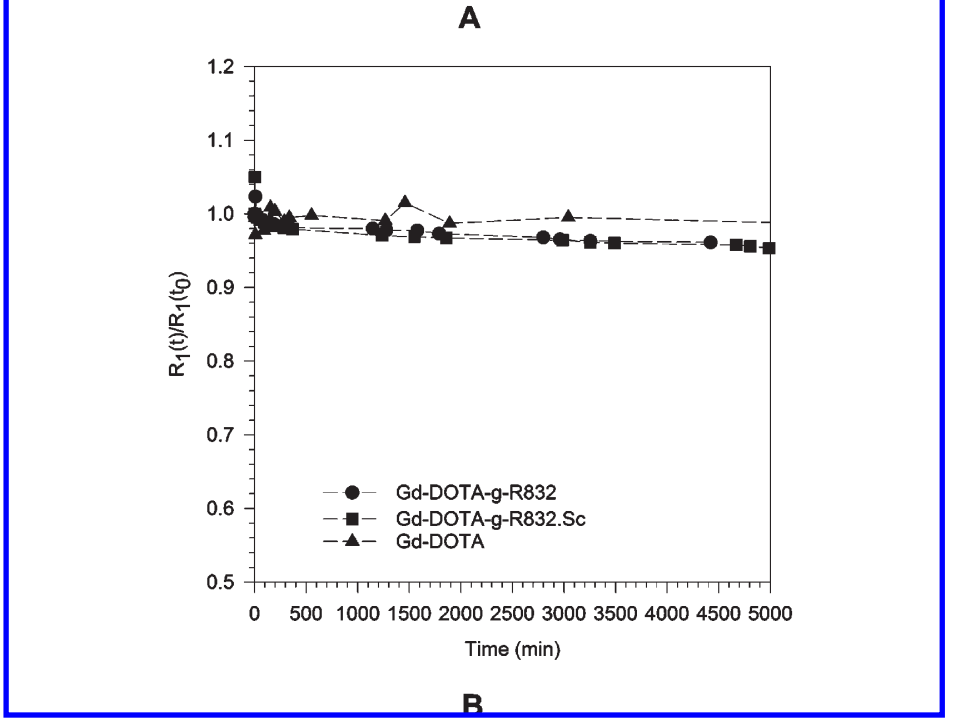

Figure 3. Physicochemical characterization of Gd-DOTA-R832 and of Gd-DOTA-R832.sc: (A) NMRD profiles at 310 K in comparison with Gd-DOTA; (B) evolution of the paramagnetic proton relaxation rate during transmetalation.

40 expressing the peptide C-NNSKSHT-C (encoded as R832) presented the more efficient interaction with VCAM-1, and this was confirmed after peptide synthesis and evaluation.

On the basis of the above tests of affinity, peptide R832 was conjugated to Gd-DOTA and assessed by MRI on a well documented model[42,43] of T cell mediated hepatitis characterized by VCAM-1 expression, induced in mice by ConA. This

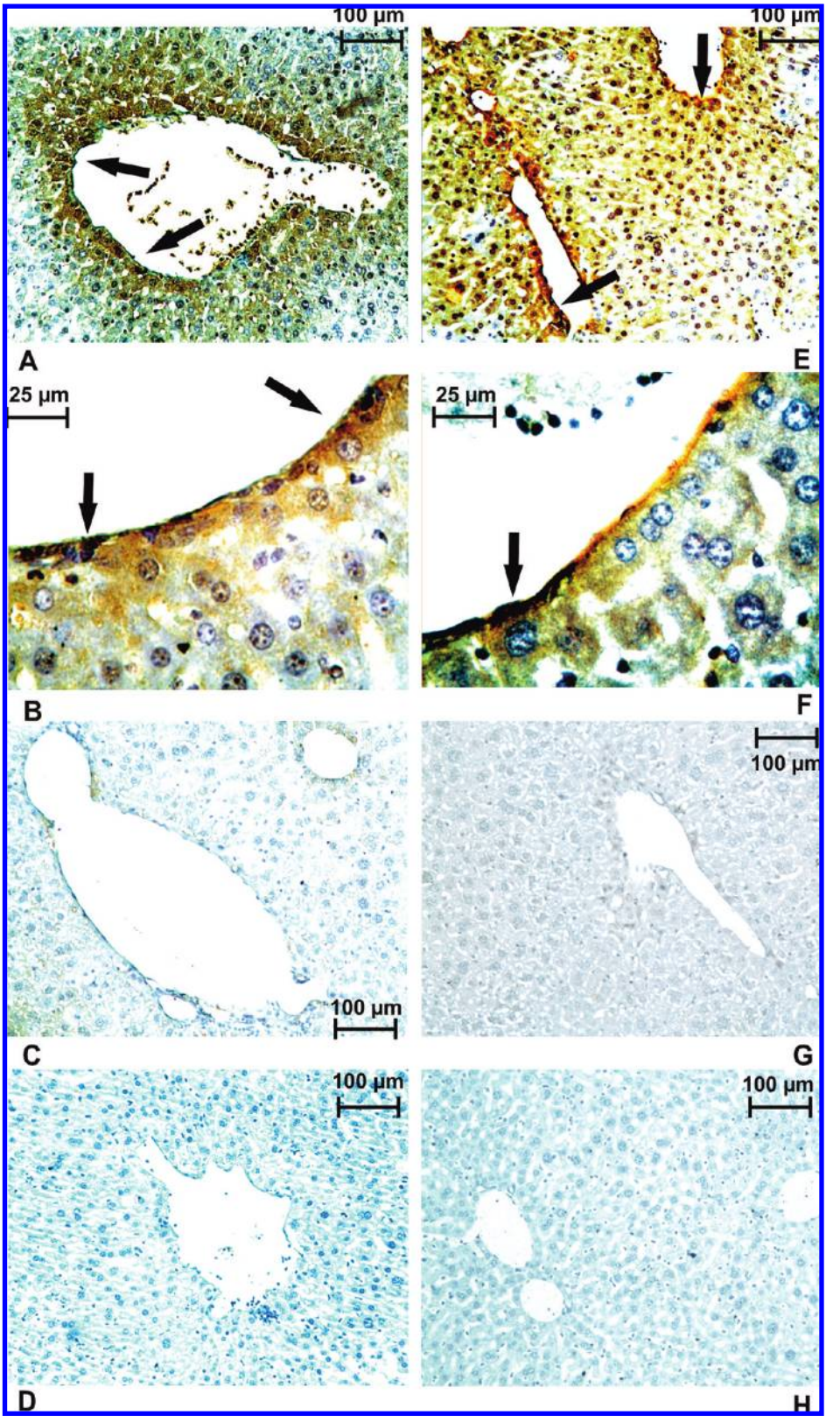

Figure 4. Immunostaining of VCAM-1 expression (stained in brown; arrows) by using R832-Bt (A−C) or anti-VCAM-1 antibody (E−G) in histologic sections of mouse liver with ConA hepatitis (6 h and 45 min after ConA injection; A, B, E, F) and of healthy liver (C, G). The larger magnifications shown in parts B and F are focused on the vascular endothelium. The negative controls (D, H) show that secondary antibodies did not interfere with the specific immunostaining.

evaluation aimed at confirming the VCAM-1 targeting with our molecular imaging probe, which subsequently served for the detection of atherosclerotic plaques.

In this model of hepatitis, 4−8 h after its administration, ConA sharply enhances lymphocyte adhesion to vessel walls, which coincides with VCAM-1 expression.[41,42] The

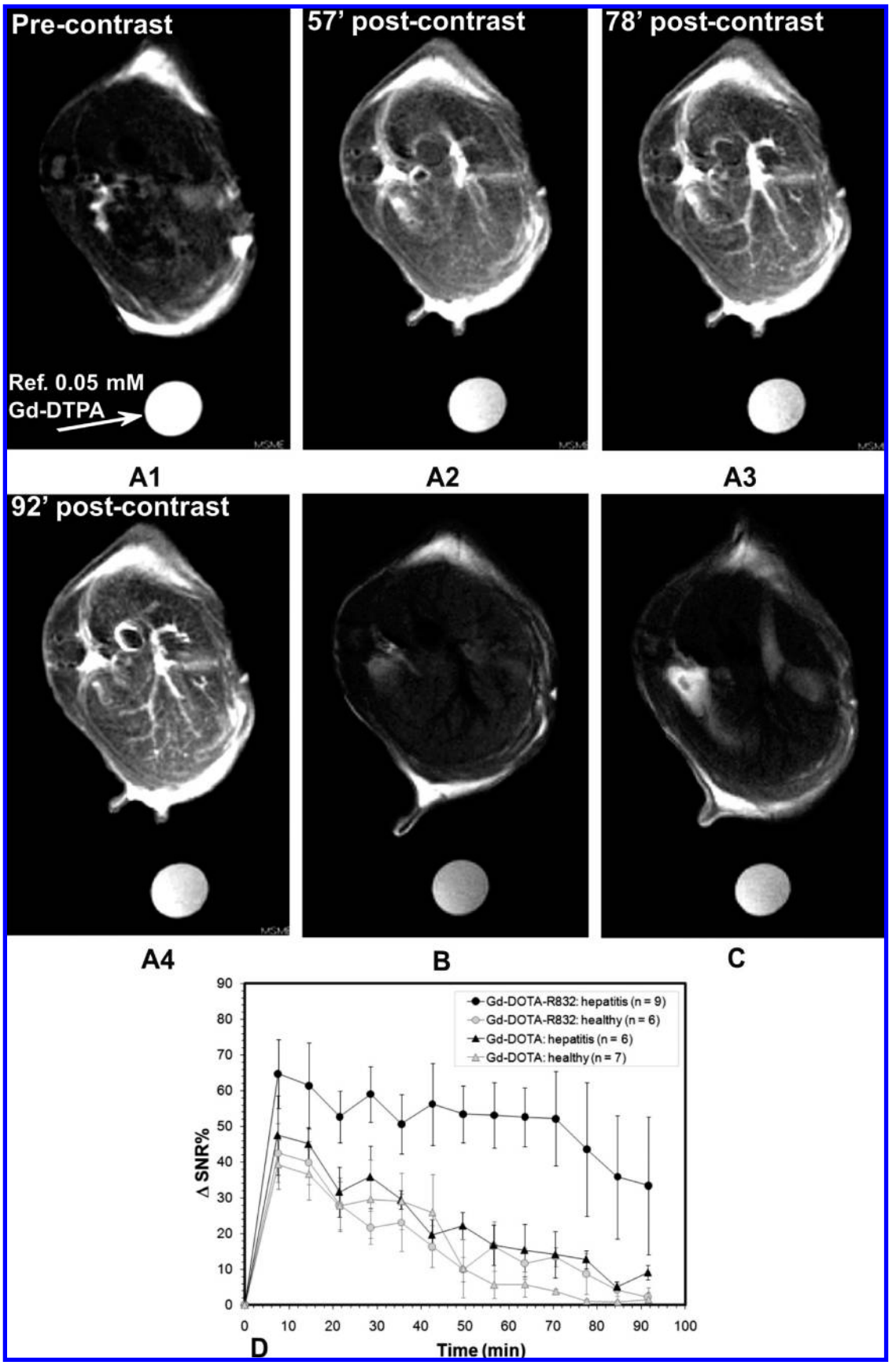

Figure 5. Molecular MRI of VCAM-1 expression in ConA hepatitis with Gd-DOTA-R832 (A1−A4) compared to 92 min postcontrast images of a healthy mouse injected with the same CA (B) and to a mouse with ConA hepatitis injected with Gd-DOTA (C). The images are axial slices acquired at the level of mouse liver and show the enhancement of the branches of the portal system. The ΔSNR% produced in liver by the two CAs is shown in part D, where the results are represented as the mean ± SEM.

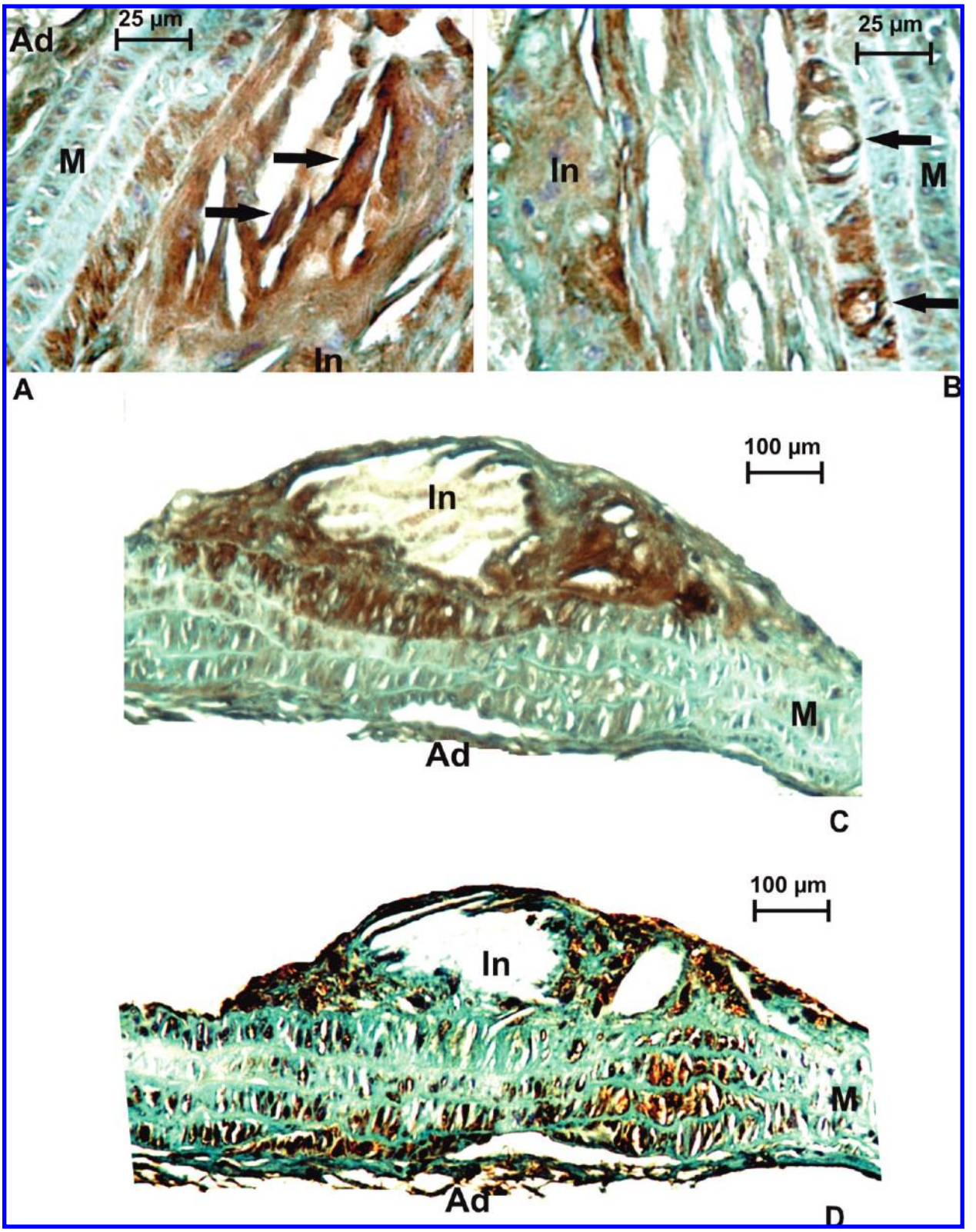

Figure 6. Immunostaining of VCAM-1 expression in longitudinal histological sections of abdominal aorta from ApoE$^{-/-}$ mice. Staining with anti-VCAM-1 antibody (stained in brown; A, B) shows high expression both in intima (In) and in media (M) with possible development of angiogenic neovessels (pointed by arrows). Ad stands for adventitia. VCAM-1 expression as detected by anti-VCAM-1 antibody (C) is colocalized with R832-Bt immunostaining (D) in the same area of abdominal aorta.

CAMs (i.e., E-selectin, VCAM-1, and ICAM-1) play critical roles in lymphocyte adhesion to ECs and their migration into the interstitial hepatic tissue. Increased number of adhering lymphocytes was widely observed in the hepatic vasculature including periportal and centrolobular sinusoids, central veins, sublobular veins, and small hepatic veins. Among these veins, the sublobular veins showed the most frequent lymphocyte adhesion. In the sinusoids,

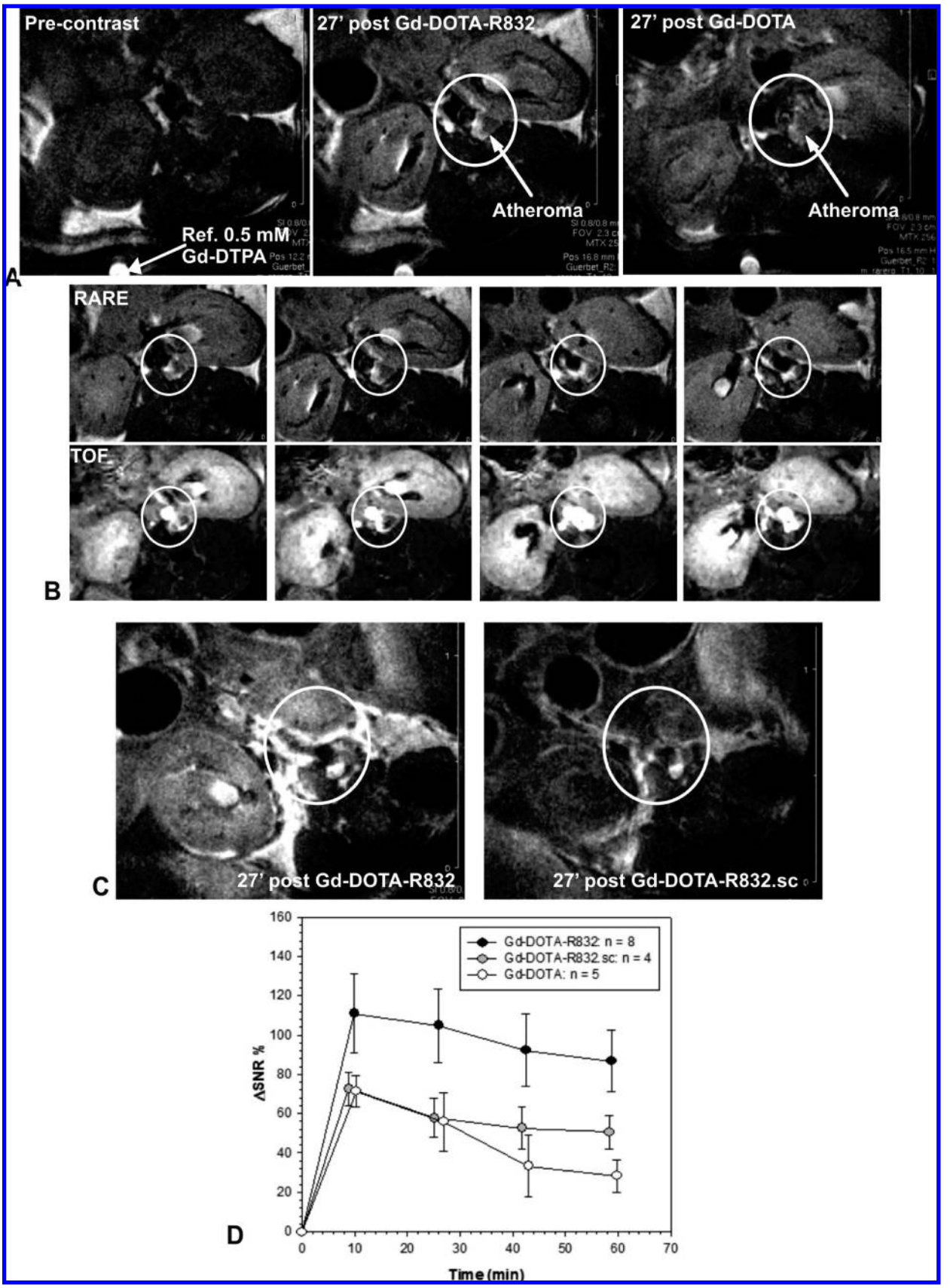

Figure 7. Molecular MRI of VCAM-1 expression in abdominal aorta of ApoE$^{-/-}$ mice. The images acquired 27 min post Gd-DOTA-R832 are compared to those obtained after Gd-DOTA administration (A). The MRI serial slices of abdominal aorta shown in part B were acquired 27 min after Gd-DOTA-R832 by RARE and TOF imaging protocols. Comparative images acquired with Gd-DOTA-R832 and with Gd-DOTA-R832.sc are presented in part C, which shows the renal artery arising off the abdominal aorta. The ΔSNR% measured on RARE images of atherosclerotic plaque of abdominal aorta is shown in part D, where the results are represented as the mean ± SEM.

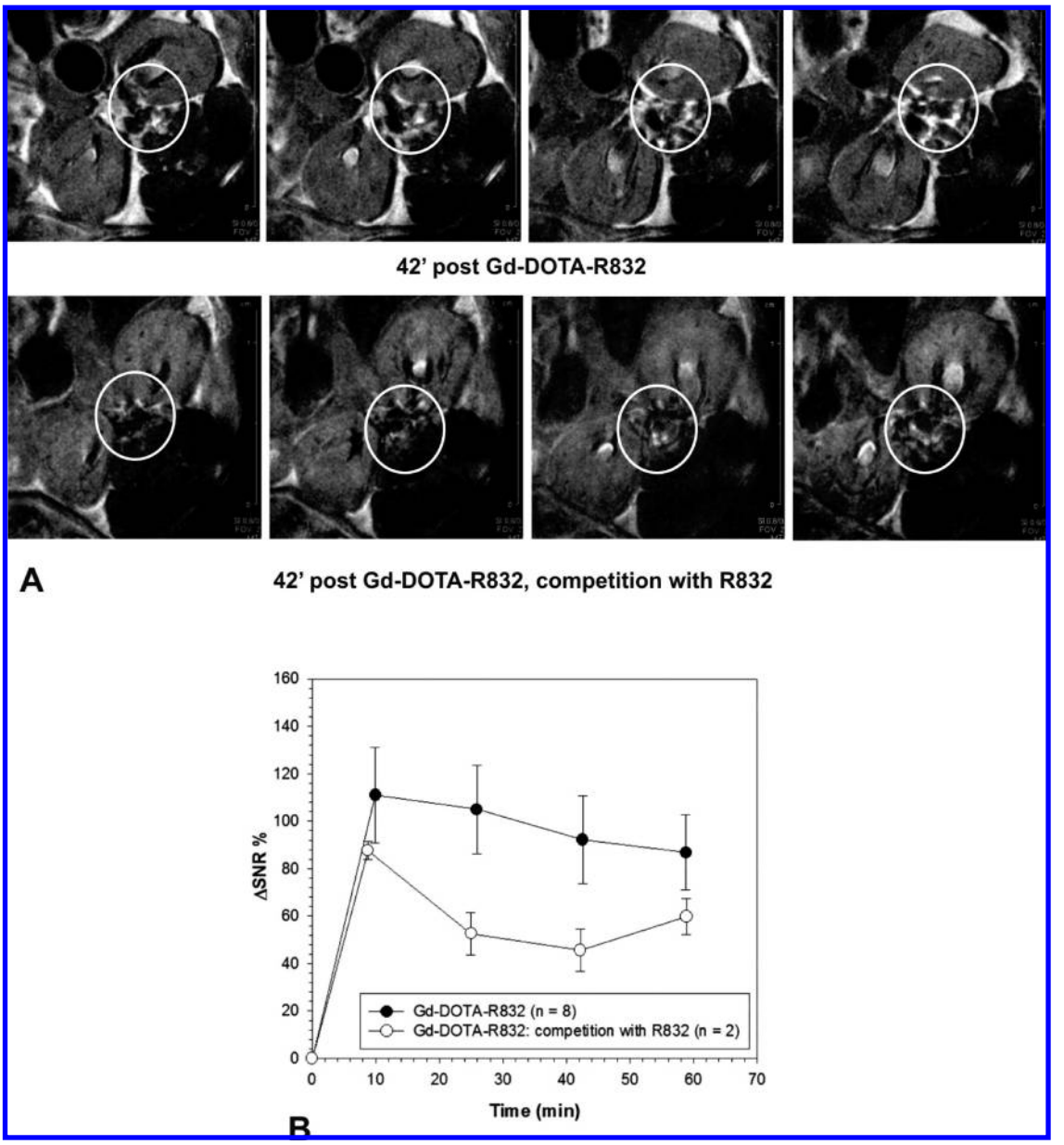

Figure 8. MRI serial slices of abdominal aorta of ApoE$^{-/-}$ mice acquired 42 min after Gd-DOTA-R832 are compared in the absence and in the presence of the competitor R832 (A). The ΔSNR% measured on images of atherosclerotic plaque is shown in part B, where the results are represented as the mean ± SEM.

lymphocytes adhered to endothelial cells and often made a close association with Kupffer cells.

VCAM-1 expression was confirmed in our experimental conditions and was colocalized with R832-Bt immunostaining of hepatic tissue around the vein lumen. As described in the literature,[44] the pattern of VCAM-1 expression was not limited to the ECs, but it probably concerned the hepatocytes and Kupffer cells as well.

The MR images evidenced an individual variability of the signal enhancement in pathological conditions induced by ConA, probably related to the timing of VCAM-1 expression. Despite this variability, we could observe the prominent delineation of the portal vein and of its branches achieved in the presence of Gd-DOTA-R832, which suggests a specific targeting of VCAM-1 expressed in these pathological conditions. Such a particular delineation of the liver blood vessels could not be noticed in healthy animals treated with Gd-DOTA-R832 or in the experimental groups that received the nonvectorized compound Gd-DOTA.

The ApoE$^{-/-}$ model of atherosclerosis studied in the present work was characterized by an extensive VCAM-1 expression, which was observed on the endothelium of atherosclerotic lesions, in subendothelial intimal tissue, and in medial layer. Capillary-like structures (that could be of angiogenic nature) surrounded by intense VCAM-1 immunostaining were observed in media and at the intima-media border, in agreement with earlier observations.[11] Microvessels in atherosclerotic plaque may be associated with its vulnerability because they can promote intraplaque hemorrhage, facilitate cholesterol deposition, support plaque growth, and sustain the influx of inflammatory cells. The plaques detected in our ApoE$^{-/-}$ mice seemed to cover the whole range of atherosclerotic pathogenesis, from fatty streaks to fibrofatty lesions; plaques with a necrotic core and thin caps were also observed.

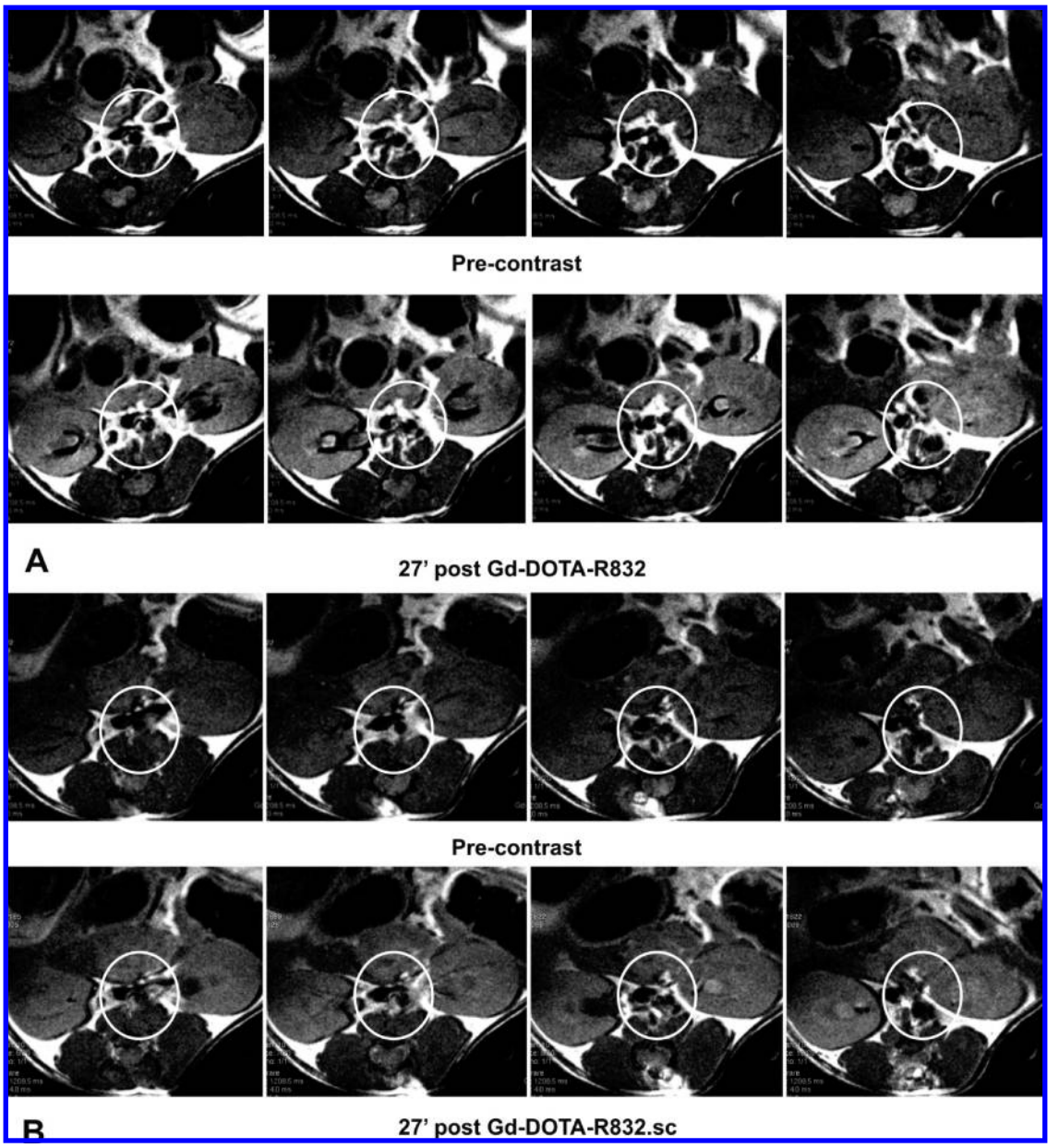

Figure 9. MRI serial slices of abdominal aorta of C57BL/6J mice acquired 27 min after Gd-DOTA-R832 (A) and Gd-DOTA-R832.sc (B).

Corroborating the reported literature,[20,45] VCAM-1 was identified in all these types of atherosclerotic lesions and it was colocalized with R832-Bt binding on histological sections.

Gd-DOTA-R832, but not Gd-DOTA-R832.sc, produced an important signal enhancement of the aortic wall in MR images, while the nonspecific contrast agent Gd-DOTA did not allow the optimal discrimination of the atheroma from the surrounding tissues. The specific VCAM-1 targeting in atherosclerotic plaque is suggested by the images obtained after preinjection of peptide R832, which attenuated the positive contrast produced by Gd-DOTA-R832. In addition to this, no particular enhancement of the aortic wall could be observed in control mice either with Gd-DOTA-R832 or with Gd-DOTA-R832.sc.

To conclude, the in vivo and in vitro evaluation of R832 suggests a specific interaction with VCAM-1 of this phage display-derived peptide binder, which could help in the diagnosis of atherosclerotic disease, both during its precocious stages and later, when the plaque is prone to rupture and thrombosis. The distinction between various plaque stages is feasible by MRI, which offers an adequate anatomical resolution for plaque morphometry. The applications of our VCAM-1-targeted contrast agent are not limited to the imaging of atherosclerotic lesions, as it also represents a potentially useful molecular imaging probe for the diagnosis and therapy monitoring of other inflammation-related pathologies, such as cancer, autoimmune diseases, and infections. As explained above, the inherent low sensitivity may represent the major limitation of VCAM-1 detection by MRI with low molecular weight paramagnetic imaging probes as that developed in the present study. This means that some areas of inflamed tissues characterized by low level of VCAM-1 expression may not attain the detection limit of MRI technology. Several strategies could be envisaged to overcome this limitation. A possible strategy is represented by the complexation of our imaging probe with radioisotopes, followed by their implementation in nuclear medicine, which has a superior sensitivity when compared to MRI. Regarding the

former imaging approach, Sans et al.[18] and Broisat et al.[46] have reported VCAM-1 detection with ^{123}I-labeled monoclonal antibody in experimental colitis[18] and with ^{123}I- and ^{99m}Tc-labeled molecular fragment of the major histocompatibility complex-1 in Watanabe heritable hyperlipidaemic rabbits.[46] The drawback represented by the low anatomical resolution mainly in the case of atherosclerotic pathology could be surmounted by a multimodal imaging approach such as PET/CT and PET/MRI imaging systems. For more sensitive MRI applications, the peptide could be conjugated to iron oxide superparamagnetic agents, after rendering them enough furtive to circumvent the inevitable capture by the phagocytic cells of the reticuloendothelial system. Such agents were described by other authors in the context of VCAM-1 targeting, where antibody[19,23,24] or peptide[20] functionalized CLIO (cross-linked iron oxide)[19,20] or microparticles of iron oxide[23,24] were evaluated in various inflammation models. In the case of atherosclerosis imaging, these superparamagnetic agents were often validated in ex vivo models, which do not reproduce all the complex mechanisms of MRI contrast in in vivo systems that could render rather difficult the robust diagnosis of this disease. However, as previously explained, several techniques were recently developed[29,30] to convert in a positive contrast the hyposignal produced by iron oxide superparamagnetic agents and to assist thus a robust clinical diagnosis.

4. Experimental Section

4.1. Instrumentation and General Procedures. The DNA sequencing of the phage clones was performed by using an Eppendorf Personal Mastercycler (VWR International, Leuven, Belgium) and a CEQ 2000 XL DNA analysis system (Beckman CoulterTM, Analis, Namur, Belgium). To evaluate the affinity for the target of the phage clones and of the synthesized peptides, a microplate washer (Adil Instruments LP21, Fisher-Bioblock, Tournai, Belgium) was used to wash the wells of the ELISA plates, while an automatic incubator/shaker (Heildorf Instruments Titramax 1000, Fisher-Bioblock Scientific, Tournai, Belgium) was employed for the incubation steps carried out with plate agitation; the OD_{405} was measured using a microplate reader (StatFax-2100, Awarness Technology, Fisher Bioblock Scientific). During the CAs synthesis, the reaction was monitored by HPLC on a Waters 600 multisolvent delivery system equipped with a Rheodyne injection valve (20 μL loop) and controlled by the Millenium software (Waters, Zellik, Belgium). The purity of the Gd-DOTA-R832/R832.sc was confirmed by HPLC (>95%). The HPLC conditions were as follows: 1 mL/min, mobile phase solvent A, water/HCOOH 0.05%; solvent B, MeOH/HCOOH 0.05%, 2−100% B in 10 min, 100% B during 2 min, 100−2% in 2 min; detection at 210 and 254 nm. The mass spectra were recorded on the Q-tof-2 (Micromass, Manchester, U.K.). The samples (1 mg) were dissolved in a mixture of methanol/water (50/50) and infused at a rate of 5 μL/min. The NMRD curves were obtained on Stelar (PV, Mede, Italy). Additional relaxation rates at 0.47, 1.4, and 7.05 T were obtained on Minispec Mq-20 and Mq-60 (Bruker, Karlsruhe, Germany). Fitting of the ^{1}H NMRD was performed with a data-processing software that uses different theoretical models describing nuclear relaxation phenomena (Minuit, CERN Library).[47,48] Transmetalation by zinc(II) ions was evaluated by the decrease of the water longitudinal relaxation rate at 310 K and 20 MHz (Bruker Minispec Mq-20) of buffered phosphate solutions (pH 7) containing 2.5 mM of the gadolinium complex and 2.5 mM of Zn.[38] The in vivo MRI studies were performed on a 200 MHz (4.7 T) Bruker imaging system (Bruker, Ettlingen, Germany). The pictures of histological samples were acquired with a Leica DFC 290 camera (Leica Microsystems, Groot Bijgaarden, Belgium).

4.2. Phage Display Experiment. 4.2.1. Panning of Phage Display Library against VCAM-1. The random disulfide-constrained cyclic heptapeptide phage display library (Ph.D.-C7C, New England BioLabs, Westburg, Leusden, The Netherlands) was panned against recombinant mouse VCAM-1/Fc chimera (R&D Systems, Abington, U.K.), which was immobilized alternatively on Dynabeads Protein A or G (Dynal Biotech, Compiègne, France) during the four rounds of biopanning. The phage library was preincubated with target-free Dynabeads and then with Dynabeads coated with VCAM-1 (46 nM). The eluted phage pool was amplified by *E. coli* (K12 ER2738, New England BioLabs) infection.

4.2.2. Sequencing of the Phage Clones. Phage DNA was isolated and purified by phenol extraction−ethanol precipitation. The sequence reaction (Mastercycler Personal) was carried out by the Sanger method, using the Quick Start Kit (Beckman Coulter, Analis, Namur, Belgium) and a 20-base primer ($^{5'}$CCCTCATAGTTAGCGTAACG$^{3'}$) (New England BioLabs). The DNA sequence was analyzed on a CEQ 2000 XL DNA analysis system. Sequence reading was performed automatically by using the JaMBW 1.1 software (http://bioinformatics.org/JaMBW/). Peptide sequences were aligned with BLAST (The Basic Local Alignment Search Tool).

4.2.3. Evaluation of the Phage Clones. 4.2.3.1. Affinity for Recombinant Mouse and Human VCAM-1. Before VCAM-1 immobilization on Reacti-Bind Protein A coated plates (Pierce, Perbio Science, Erembodegem, Belgium), the wells were washed three times with TBS-T buffer (50 mM Tris-HCl, 150 mM NaCl, pH 7.5, 0.5% Tween-20); all the washing steps were performed automatically with a microplate washer. VCAM-1 (10 μg/mL) was diluted in the immobilization buffer (50 mM Tris-HCl, 150 mM NaCl, pH 7.4), and an amount of 0.2 mL was transferred per well to be tested. For immobilization, the plates were incubated for 60 min at room temperature with moderate agitation (300 rpm, Heildorf Instruments Titramax 1000), and wells were then washed three times as described above. The plates are preblocked and ready to use, so their blocking is not necessary.

The phage clones were diluted to 10^{12} virions/0.1 mL of modified TBS (TBSM) buffer (50 mM Tris-HCl, 150 mM NaCl, 1 mM $CaCl_2$, 1 mM $MgCl_2$, 2 mM $MnCl_2$, 10 mM Hepes, pH 7.4) completed with 0.5% Tween-20 (TBSM-T), and incubated with VCAM-1 coated wells at 37 °C, 2 h, under moderate agitation. After the wells were washed 6 times with TBSM-T, the HRP-conjugated anti-M13 antibody (Amersham Pharmacia Biotech Benelux, Roosendaal, The Netherlands) was diluted 1:5000 in TBSM completed with 5 mg BSA/mL, and 0.2 mL/well of this solution was incubated at room temperature for 1 h under moderate agitation. The plate was then washed 6 times with TBSM-T buffer, and 0.2 mL/well of ABTS [2,2′-azino-bis(3-ethylbenzthiazoline-6-sulfonic acid), diamonium salt (Sigma-Aldrich, Bornem, Belgium)] solution (22 mg ABTS in 100 mL of 50 mM sodium citrate, pH 4.0) completed with 0.05% H_2O_2 was added. The OD_{405} was measured using a microplate reader (StatFax-2100).

4.2.3.2. Competition Tests. Culture of HUVEC. For the ELISA tests of competition, HUVEC (kind gift from V. Castronovo, ULG, Belgium) were seeded on 96-well microculture plates by transferring 0.1 mL of 2×10^4 cells/mL. The plates were incubated at 37 °C in a humidified 5% CO_2 incubator until confluent. They were then stimulated with 10 ng/mL of TNFα (Alexis Biochemicals, Zandhoven, Belgium) for 5 h (37 °C, 5% CO_2); control cells were left nonstimulated.

Culture of Jurkat T Lymphocytes. Jurkat cells were cultured (37 °C in a humidified 5% CO_2 incubator) at a concentration of less than 1×10^6 cells/mL in RPMI-1640 culture medium (Sigma-Aldrich) supplemented with 10% newborn calf serum heat inactivated and antibiotic−antimycotic (both from Invitrogen, Merelbeke, Belgium). The cells were stimulated with 50 ng/mL phorbol 12-myristate 13-acetate (PMA, Sigma-Aldrich) for 3 h (37 °C, 5% CO_2).

ELISA Protocol. HUVEC coated wells of microtitration plates (CELLCOAT collagen type I, Greiner, Wemmel, Belgium) were rinsed 3 times with 0.2 mL of cold PBS. After fixation (5 min, 4 °C) with 1% glutaraldehyde in phosphate buffer, pH 7.5, the cells were rinsed 3 times with 0.2 mL of cold PBS and the wells were then blocked (1 h, 4 °C) with 0.2 mL of 5 mg/mL BSA in PBS.

HUVEC were incubated with phages or Jurkat cells according to the following experimental protocol:

(A) Control HUVEC were incubated (40 min, 4 °C) with 0.1 mL of 10^{13} virions in TBSM completed with 0.1% BSA (TBSM-B).

(B) TNF-α-stimulated HUVEC (HUVEC/TNFα) were incubated (40 min, 4 °C) with 0.1 mL of 10^{13} virions in TBSM-B.

(C) Several wells (corresponding to the number of clones to be tested) coated with HUVEC/TNFα were filled with 0.1 mL of TBSM-B.

(D) 10^{13} virions were incubated with 0.1 mL of VCAM-1 (10 μg/mL in TBSM-B) in previously blocked wells (5 mg/mL BSA in 0.1 M $NaHCO_3$, 0.02% NaN_3, pH 8.6) for 20 min at 4 °C.

(E) The second group of HUVEC/TNFα wells (corresponding to the number of clones to be tested) were incubated with 0.05 mL of 10^{13} virions [in TBSM-B completed with 2 mM glucose (TBSM-BG)] for 20 min at 4 °C.

(F) The third group of HUVEC/TNFα wells (corresponding to the number of clones to be tested) were incubated with 0.05 mL of 1.5×10^5 Jurkat cells in TBSM-BG for 20 min at 4 °C.

The phages or Jurkat cells were then added to the wells C, E, and F as follows:

(a) The solution of the D wells was transferred to the C wells.

(b) An amount of 0.05 mL of 1.5×10^5 Jurkat cells in TBSM-BG was added to the E wells.

(c) An amount of 0.05 mL of 10^{13} virions in TBSM-BG was added to the F wells.

After incubation for 20 min at 4 °C, the wells were rinsed 3 times with 0.2 mL of cold TBSM, and then they were incubated with 0.2 mL of HRP-conjugated anti-M13 antibody diluted in cold TBSM (containing 5 mg BSA/mL) for 30 min at 4 °C. The wells were subsequently rinsed 3 times with 0.2 mL of cold TBSM, and 0.2 mL of ABTS/H_2O_2 solution was added. The OD_{405} was measured using a microplate reader.

Evaluation of VCAM-1 Expression by HUVEC. VCAM-1 expression on HUVEC was confirmed with mouse antihuman VCAM-1 monoclonal antibody (clone BBIG-V1, 4B2; R&D Systems) and peroxidase-conjugated antimouse IgG (Sigma-Aldrich). After cell fixation and plate blocking as described, anti-VCAM-1 antibody was diluted to 1 μg/mL in PBS completed with 5 mg/mL of BSA, and 0.2 mL/well of this solution was incubated 1 h at 4 °C. Subsequently, the wells were washed 3 times with 0.2 mL/well of PBS, and then peroxidase-conjugated antimouse IgG (0.2 mL/well diluted 1:500 in PBS completed with 5 mg/mL of BSA) was added and incubated 30 min at 4 °C. After the samples were washed 3 times with PBS, the color reaction was developed by using the ABTS substrate solution as described and the OD_{405} was measured.

4.3. Characterization of the Selected VCAM-1-Binding Peptides. Four peptides were selected for synthesis (NeoMPS, Strasbourg, France) and subsequent evaluation. For convenience, the peptides were encoded as follows: R831 (clone 41, C-MKTDTRL-C), R832 (clone 40, C-NNSKSHT-C), R833 (clone 22, C-HLGARTH-C), R834 (clone 10, C-RTTSDAL-C). The purity of the commercial biotinylated peptides as determined by HPLC at NeoMPS was as follows: >80% for R831, >70% for R832, >90% for R833, and >80% for R834.

4.3.1. Estimation of K_d. Human recombinant VCAM-1 (R&D Systems) was immobilized (0.1 mL/well, overnight, 4 °C) at a concentration of 10 μg/mL in 0.1 M $NaHCO_3$, pH 8.6. Next day, the wells were blocked with 0.3 mL/well of blocking buffer (0.1 M $NaHCO_3$, 0.02% NaN_3, 1% BSA) for 2 h at 4 °C. The wells were then rinsed 5 times with 0.2 mL/well of TBSM-T (Tween-20 concentration of 0.05%).

Serial dilutions of biotinylated peptides were prepared in TBSM, and 0.1 mL of each peptide dilution was transferred to VCAM-1-coated wells followed by an incubation of 2 h at room temperature. The wells were rinsed 5 times with TBSM-T and subsequently were incubated 1 h at 4 °C with 0.2 mL/well of streptavidin ABC complex/peroxydase (DakoCytomation SAS, Trappes, France). The ABC complex solution was discarded, and wells were rinsed four times with TBSM-T. The staining reaction was developed with 0.1 mL/well of ABTS/H_2O_2, and OD_{405} was measured with a microplate reader.

4.3.2. Inhibition of Cell Adhesion to VCAM-1 and Estimation of IC_{50}. VCAM-1 (20 μg/mL) immobilization on ELISA plates, the blocking of wells, and Jurkat cell stimulation were performed as described above.

Each peptide (not biotinylated; 8.8×10^{-3} to 8.8×10^{-8} M) or the monoclonal antihuman VCAM-1 antibody (6.7×10^{-7} to 1.05×10^{-8} M), used as a reference compound, was preincubated (room temperature, 1 h) with VCAM-1 coated wells. Jurkat cells (10^5 cells/well) were then added in the presence or in the absence of the competitor molecule, and the samples were incubated for another 1 h. After the wells were washed 3 times, the cells bound to VCAM-1 were fixed (4 °C, 45 min) with 0.05 mL/well of 1% glutaraldehyde in PBS and stained for 30 min with crystal violet (1% crystal violet in 10% ethanol). After being rinsed with distilled water, the samples were incubated with destaining solution (33% ethanol) and the OD_{570} was measured.

4.3.3. In Vivo MRI Evaluation of VCAM-1-Targeted Paramagnetic Contrast Agents. 4.3.3.1. Contrast Agents: Synthesis of the Gd Complexes. Peptide R832 and its scrambled homologue (HSCNKNSCT; R832.sc) were synthesized at NeoMPS. The purity of the synthesized commercial peptides was >80% as determined by HPLC at NeoMPS. Other commercial products were purchased from Sigma-Aldrich. Protected peptides (lysines with TFA groups) were conjugated to Gd-DOTA-diethylsquarate, which was prepared just before use from Gd-aminobutyl-DOTA and diethylsquarate (Scheme 1). Gd-aminobutyl-DOTA was obtained as previously described.[49] The purity of the Gd-DOTA-R832/R832.sc was confirmed by HPLC (>95%).

Synthesis of Gd-DOTA-Diethylsquarate. An amount of 500 mg of Gd-aminobutyl-DOTA was suspended in 7 mL of anhydrous DMSO under argon atmosphere. Then 0.139 g of Et_3N and 0.345 g of diethylsquarate were added. The mixture was stirred 1 h at room temperature. A total of 35 mL of ether was added, and a viscous yellow oil was obtained. This oil was treated 2 times with 25 mL of ether. The solid was filtered and washed with CH_2Cl_2.

Synthesis of Gd-DOTA-R832/R832.sc. An amount of 210 mg of Gd-DOTA-diethylsquarate was solubilized in 15 mL of water. A saturated solution of K_2CO_3 was added to this solution in order to adjust the pH to 8.5. A total of 350 mg of protected peptide (TFA group on the lysine residue) was added, and the pH was maintained at 8.5, while the mixture was stirred during 4 days. The reaction was monitored by HPLC using a Novapac column (Waters).

The peptide was deprotected by hydrolysis at pH 9.5 in an alkaline aqueous solution of K_2CO_3, and the mixture was stirred during 2 h at room temperature. After completing the reaction, the pH was adjusted to 7 using 6 M HCl. The mixture was dialyzed (membrane cutoff = 1000) during 48 h, then chromatographed on reverse phase RP-18 (MeOH/water (50/50)). HPLC: t_R (Gd-DOTA-diethylsquarate) = 2.30, t_R (Gd-DOTA-R832) = 5.4, t_R (Gd-DOTA-R832.sc) = 5.5. ESI-MS, $[M + H]^+$: 949 $(M + 3Na)^{2+}$; 960 $(M + 4Na)^{2+}$. ESI-MS, Gd-DOTA-R832: M_{mes} = 949.2766, M_{calc} = 949.2657 ($C_{65}H_{97}N_{20}O_{28}S_2Na_3Gd$). ESI-MS, Gd-DOTA-R832.sc: M_{mes} = 949.2542, M_{calc} = 949.2657 ($C_{65}H_{97}N_{20}O_{28}S_2Na_3Gd$).

4.3.3.2. Animal Studies. The experiments fulfill the requirements of the Ethical Committee of our institution. The mice

Scheme 1. Synthetic Scheme of Gd-DOTA Compounds

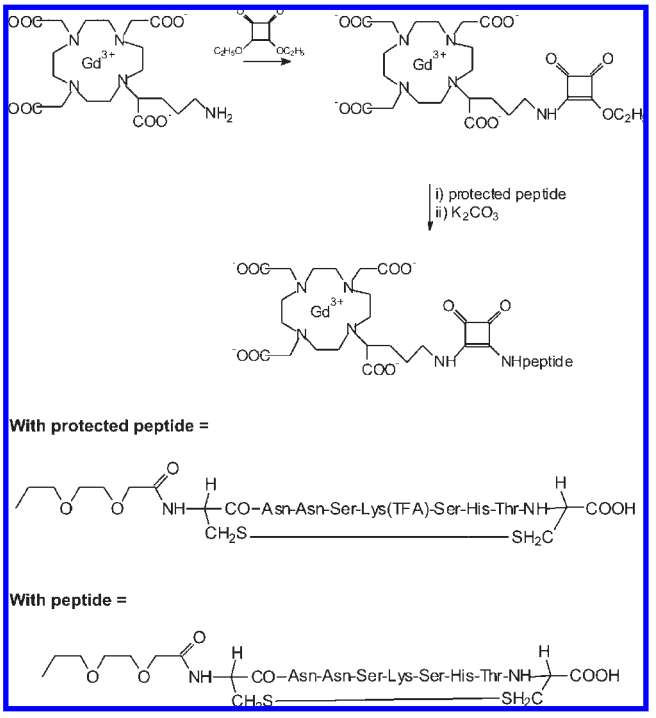

were anesthetized with 50 mg/kg bw, ip, of Nembutal (Sanofi, Brussels, Belgium). All the experiments were performed on a 200 MHz (4.7 T) Bruker imaging system equipped with a vertical magnet and a microimaging device (Micro2.5AHS/RF, 25 mm coil). Gd-DOTA (Dotarem) was used as a nonspecific CA. The CAs were injected iv (caudal or femoral veins) at a dose of 0.1 mmol/kg bw. In the case of ApoE$^{-/-}$ mice, a competition experiment was carried out by preinjecting (~15 min before Gd-DOTA-R832) the nonconjugated peptide R832 at a dose of 0.12 mmol/kg bw.

ConA Hepatitis. Before induction of hepatitis, the Balb/c mice (average weight 26 g, Harlan, Horst, The Netherlands) were anesthetized with Nembutal diluted to 1:5 with physiological salt; anesthesia was repeated ~1.5 h after the induction of hepatitis by using the same diluted solution of Nembutal. Hepatitis was induced by the iv (caudal vein) injection of 20 mg/kg of freshly prepared ConA (Sigma-Aldrich); the solution prepared with 0.5 mg ConA dissolved in 150 μL of physiological salt (0.9% NaCl) was injected in a mouse of 25 g.

On the basis of published data,[27,28] VCAM-1 is intensely expressed at 4−8 h after ConA injection. The MRI protocol was, therefore, scheduled according to VCAM-1 expression as follows: (1) the precontrast MRI session started 4 h and 30 min after ConA injection; (2) the CA was injected at ~5 h after ConA injection; (3) postcontrast MR images were acquired every 7 min for ~1 h and 30 min (up to about 6.5−7 h after ConA injection).

The images were acquired with a multislice−multiecho (MSME) sequence (TR/TE = 307.4/14.7 ms, matrix = 256, no. of averages = 4, FOV = 5 cm, slice thickness = 3 mm, 8 axial slices, TA = 5 min 14 s).

SI was measured in regions of interest (ROIs) drawn globally on each slice of the liver and in a region situated out of the image of the animal, representing the standard deviation (SD) of noise. SI enhancement (ΔSNR%) was calculated according to the following equation:

$$\Delta\mathrm{SNR}\% = \frac{(\mathrm{SI_{post}}/\mathrm{NoiseSD}) - (\mathrm{SI_{pre}}/\mathrm{NoiseSD})}{(\mathrm{SI_{pre}}/\mathrm{NoiseSD})} \times 100$$

where $\mathrm{SI_{post}}$ = postcontrast SI and where $\mathrm{SI_{pre}}$ = precontrast SI.

Atherosclerosis (ApoE$^{-/-}$ Mice). Female C57Bl ApoE^{tm1unc} mice, aged ~15 months, were obtained from Guerbet's animal facility. The animals received a Western diet (0.21% cholesterol) for 3 months prior to the MRI studies. Control, healthy animals were represented by C57BL/6J mice (Harlan).

Images were acquired at the level of abdominal aorta as described earlier[11] with RARE imaging protocol (TR/TE = 1048.5/4 ms, RARE factor = 4, NEX = 4, matrix = 256 × 256, FOV = 2.3 cm, slice thickness 0.8 mm, 20 axial slices, spatial resolution = 90 μm, TA = 4 min and 28 s). A 3D-TOF sequence (TR/TE = 10/2 ms, flip angle = 20°, NEX = 2, FOV = 4 cm × 2 cm × 4 cm, matrix = 256 × 128 × 64, slice thickness = 1 mm, 60 axial slices, spatial resolution = 156 μm × 156 μm × 625 μm, TA = 2 min 43 s) was used with the aim to confirm the anatomical location of the aorta in the image slice.

SI values for each time point were measured within ROIs drawn manually by using the OSIRIS image analysis software in the arterial wall of the abdominal aorta. The ROIs were drawn on serial slices on the area of signal enhancement around the vessel lumen and were reproduced for precontrast images, where the aortic wall was not discriminated from the surrounding tissue. The noise SD was also measured in a region situated out of the animal's image. SI enhancement (ΔSNR%) was calculated as described above.

The data were averaged, and SEM was calculated for each time point.

Immunohistochemistry of VCAM-1 Expression and Colocalization with Biotinylated R832 Immunostaining. The samples of liver (ConA and healthy Balb/c mice) and aorta (ApoE$^{-/-}$) were fixed by immersion in a Bouin's solution (aortas) or buffered 4% paraformaldehyde (livers). After routine processing and paraffin embedding, 5 μm thick sections were cut.

After rehydration of histological samples, endogenous peroxidases were blocked with 0.15% H_2O_2, while endogenous biotin was blocked with a blocking kit (Invitrogen). VCAM-1 expression was detected by overnight incubation with 2 μg/mL of rabbit anti-VCAM-1 polyclonal antibody (Santa Cruz Biotechnology, Heidelberg, Germany), followed by 1 h of incubation with 10 μg/mL of biotinylated goat antirabbit IgG (Vector Labconsult, Brussels, Belgium) and streptavidin-linked peroxydase complexes (ABC kit, DakoCytomation). Finally, the sections were incubated for 5 min with 50 mM Tris-HCl, pH 7.4, and then stained with 0.05% 3,3′-diaminobenzidine (DAB) completed with 0.02% H_2O_2 in PBS. The sections were finally counterstained with hemalun and Luxol fast blue and mounted in a permanent medium.

R832-Bt prepared in TBSM was incubated overnight at a concentration of 1 μM for liver samples and of 0.2 μM for aorta samples. The peptide bound to the samples was detected with 5 μg/mL of goat antibiotin IgG and with 1 μg/mL of horse peroxidase-conjugated antigoat IgG (both from Vector Labconsult). The staining, counterstaining, and mounting were performed as described above.

Acknowledgment. The authors thank Patricia de Francisco for her help in preparing the manuscript and Annik Maes and Oltea Murariu for their technical assistance in immunohistochemistry studies. The FNRS program is gratefully acknowledged for the upgrade of the AVANCE-200 imaging system.

Supporting Information Available: Experimental procedures for the panning of phage display library (including information about phage display library and *E. coli* host strain) against VCAM-1. This material is available free of charge via the Internet at http://pubs.acs.org.

References

(1) Ou, R.; Zhang, M.; Huang, L.; Flavell, R. A.; Koni, P. A.; Moskophidis, D. Regulation of immune response and inflammatory reactions against viral infection by VCAM-1. *J. Virol.* **2008**, *82*, 2952–2965.

(2) Libby, P. Inflammation and cardiovascular disease mechanisms. *Am. J. Clin. Nutr.* **2006**, *83* (Suppl.), 456S–460S.
(3) Davis, C.; Fischer, J.; Ley, K.; Sarembock, I. J. The role of inflammation in vascular injury and repair. *J. Thromb. Haemostasis* **2003**, *1*, 1699–1709.
(4) Libby, P. Inflammation in atherosclerosis. *Nature* **2002**, *420*, 868–874.
(5) Ley, K.; Huo, Y. VCAM-1 is critical in atherosclerosis. *J. Clin. Invest.* **2001**, *107*, 1209–1210.
(6) Libby, P.; Aikawa, M.; Schonbeck, U. Cholesterol and atherosclerosis. *Biochim. Biophys. Acta* **2000**, *1529*, 299–309.
(7) Steinberg, D. Atherogenesis in perspective: Hypercholesterolemia and inflammation as partners in crime. *Nat. Med.* **2002**, *8*, 1211–1217.
(8) Topper, J. N.; Gimbrone, M. A. Jr. Blood flow and vascular gene expression: fluid shear stress as a modulator of endothelial phenotype. *Mol. Med. Today* **1999**, *5*, 40–46.
(9) De Caterina, R.; Libby, P.; Peng, H. B.; Thannickal, V. J.; Rajavashisth, T. B.; Gimbrone, M. A. Jr.; Shin, W. S.; Liao, J. K. Nitric oxide decreases cytokine-induced endothelial activation. Nitric oxide selectively reduces endothelial expression of adhesion molecules and proinflammatory cytokines. *J. Clin. Invest.* **1995**, *96*, 60–68.
(10) de Boer, O. J.; van der Wal, A. C.; Teeling, P.; Becker, A. E. Leucocyte recruitment in rupture prone regions of lipid-rich plaques: a prominent role for neovascularization?. *Cardiovasc. Res.* **1999**, *41*, 443–449.
(11) Burtea, C.; Laurent, S.; Murariu, O.; Rattat, D.; Toubeau, G.; Verbruggen, A.; Vansthertem, D.; Vander Elst, L.; Muller, R. N. Molecular imaging of $\alpha_v\beta_3$ integrin expression in atherosclerotic plaques with a mimetic of RGD peptide grafted to Gd-DTPA. *Cardiovasc. Res.* **2008**, *78*, 148–157.
(12) O'Brien, K. D.; McDonald, T. O.; Chait, A.; Allen, M. D.; Alpers, C. E. Neovascular expression of E-selectin, intercellular adhesion molecule-1, and vascular cell adhesion molecule-1 in human atherosclerosis and their relation to intimal leukocyte content. *Circulation* **1996**, *93*, 672–682.
(13) Moiseeva, E. P. Adhesion receptors of vascular smooth muscle cells and their functions. *Cardiovasc. Res.* **2001**, *52*, 372–386.
(14) Bengel, F. M. Atherosclerosis imaging on the molecular level *J. Nucl. Cardiol.* **2006**, *13*, 111–118.
(15) Naghavi, M.; Libby, P.; Falk, E.; Casscells, S. W.; Litovsky, S.; Rumberger, J.; Badimon, J. J.; Stefanadis, C.; Moreno, P.; Pasterkamp, G.; Fayad, Z.; Stone, P. H.; Waxman, S.; Raggi, P.; Madjid, M.; Zarrabi, A.; Burke, A.; Yuan, C.; Fitzgerald, P. J.; Siscovick, D. S.; de Korte, C. L.; Aikawa, M.; Juhani Airaksinen, K. E.; Assmann, G.; Becker, C. R.; Chesebro, J. H.; Farb, A.; Galis, Z. S.; Jackson, C.; Jang, I. K.; Koenig, W.; Lodder, R. A.; March, K.; Demirovic, J.; Navab, M.; Priori, S. G.; Rekhter, M. D.; Bahr, R.; Grundy, S. M.; Mehran, R.; Colombo, A.; Boerwinkle, E.; Ballantyne, C.; Insull, W.; Schwartz, R. S.; Vogel, R.; Serruys, P. W.; Hansson, G. K.; Faxon, D. P.; Kaul, S.; Drexler, H.; Greenland, P.; Muller, J. E.; Virmani, R.; Ridker, P. M.; Zipes, D. P.; Shah, P. K.; Willerson, J. T. From vulnerable plaque to vulnerable patient: a call for new definitions and risk assessment strategies. *Circulation* **2003**, *108*, 1664–1672.
(16) Jaffer, F. A.; Libby, P.; Weissleder, R. Molecular and cellular imaging of atherosclerosis. Emerging applications. *J. Am. Coll. Cardiol.* **2006**, *47*, 1328–1338.
(17) Burtea, C.; Laurent, S.; Vander Elst, L.; Muller, R. N. Contrast Agents. Magnetic Resonance. In Handbook of Experimental Pharmacology; Semmler, W., Schwaiger, M., Eds.; Springer-Verlag: Berlin and Heidelberg, Germany, 2008; Vol. 185, Part 1, pp 135−165.
(18) Sans, M.; Fuster, D.; Vasquez, A.; Setoain, F. J.; Piera, C.; Pique, J. M.; Panes, J. ^{123}Iodine-labeled anti-VCAM-1 antibody scintigraphy in the assessment of experimental colitis. *Eur. J. Gastroenterol. Hepatol.* **2001**, *13*, 31–38.
(19) Tsurkas, A.; Shinde-Patil, V. R.; Kelly, K. A.; Patel, P.; Wolley, A.; Allport, J. R.; Weissleder, R. In vivo imaging of activated endothelium using an anti-VCAM-1 magnetooptical probe. *Bioconjugate Chem.* **2005**, *16*, 576–581.
(20) Kelly, K. A.; Allport, J. R.; Tsurkas, A.; Shinde-Patil, V. R.; Josephson, L.; Weissleder, R. Detection of vascular adhesion molecule-1 expression using a novel multimodal nanoparticle. *Circ. Res.* **2005**, *96*, 327–336.
(21) Hamilton, A. J.; Huang, S. L.; Warnick, D.; Rabbat, M.; Kane, B.; Nagaraj, A.; Klegerman, M.; McPherson, D. D. Intravascular ultrasound molecular imaging of atheroma components in vivo. *J. Am. Coll. Cardiol.* **2004**, *43*, 453–460.
(22) Laurent, S.; Forge, D.; Port, M.; Roch, A.; Robic, C.; Vander Elst, L.; Muller, R. N. Magnetic iron oxide nanoparticles: synthesis, stabilization, vectorization, physicochemical characterizations, and biological applications. *Chem. Rev.* **2008**, *108*, 2064–2110.
(23) McAteer, M. A.; Sibson, N. R.; von Zur Muhlen, C.; Schneider, J. E.; Lowe, A. S.; Warrick, N.; Channon, K. M.; Anthony, D. C.; Choudhury, R. P. In vivo magnetic resonance imaging of acute brain inflammation using microparticles of iron oxide. *Nat. Med.* **2007**, *13*, 1253–1258.
(24) McAteer, M. A.; Schneider, J. E.; Ali, Z. A.; Warrick, N.; Bursill, C. A.; von zur Muhlen, C.; Greaves, D. R.; Neubauer, S.; Channon, K. M.; Choudhury, R. P. Magnetic resonance imaging of endothelial adhesion molecules in mouse atherosclerosis using dual-targeted microparticles of iron oxide. *Arterioscler., Thromb., Vasc. Biol.* **2008**, *28*, 77–83.
(25) von Zur Muhlen, C.; Sibson, N. R.; Peter, K.; Campbell, S. J.; Wilainam, P.; Grau, G. E.; Bode, C.; Choudhury, R. P.; Anthony, D. C. A contrast agent recognizing activated platelets reveals murine cerebral malaria pathology undetectable by conventional MRI. *J. Clin. Invest.* **2008**, *118*, 1198–207.
(26) von zur Muhlen, C.; von Elverfeldt, D.; Moeller, J. A.; Choudhury, R. P.; Paul, D.; Hagemeyer, C. E.; Olschewski, M.; Becker, A.; Neudorfer, I.; Bassler, N.; Schwarz, M.; Bode, C.; Peter, K. Magnetic resonance imaging contrast agent targeted toward activated platelets allows in vivo detection of thrombosis and monitoring of thrombolysis. *Circulation* **2008**, *118*, 258–267.
(27) Neuwelt, E. A.; Várallyay, C. G.; Manninger, S.; Solymosi, D.; Haluska, M.; Hunt, M. A.; Nesbit, G.; Stevens, A.; Jerosch-Herold, M.; Jacobs, P. M.; Hoffman, J. M. The potential of ferumoxytol nanoparticle magnetic resonance imaging, perfusion, and angiography in central nervous system malignancy: a pilot study. *Neurosurgery* **2007**, *60*, 601–611.
(28) Toso, C.; Vallee, J. P.; Morel, P.; Ris, F.; Demuylder-Mischler, S.; Lepetit-Coiffe, M.; Marangon, N.; Saudek, F.; James Shapiro, A. M.; Bosco, D.; Berney, T. Clinical magnetic resonance imaging of pancreatic islet grafts after iron nanoparticle labeling. *Am. J. Transplant.* **2008**, *8*, 701–706.
(29) Cunningham, C. H.; Arai, T.; Yang, P. C.; McConnell, M. V.; Pauly, J. M.; Conolly, S. M. Positive contrast magnetic resonance imaging of cells labeled with magnetic nanoparticles. *Magn. Reson. Med.* **2005**, *53*, 999–1005.
(30) Dahnke, H.; Liu, W.; Herzka, D.; Frank, J. A.; Schaeffter, T. Susceptibility gradient mapping (SGM): A new postprocessing method for positive contrast generation applied to superparamagnetic iron oxide particle (SPIO)-labeled cells. *Magn. Reson. Med.* **2008**, *60*, 595–603.
(31) Boutry, S.; Burtea, C.; Laurent, S.; Toubeau, G.; Vander Elst, L.; Muller, R. N. Magnetic resonance imaging of inflammation with a specific selectin-targeted contrast agent. *Magn. Reson. Med.* **2005**, *53*, 800–807.
(32) Sibson, N. R.; Blamire, A. M.; Bernades-Silva, M.; Laurent, S.; Boutry, S.; Muller, R. N.; Styles, P.; Anthony, D. C. MRI detection of early endothelial activation in brain inflammation. *Magn. Reson. Med.* **2004**, *51*, 248–252.
(33) Ladner, R. C.; Sato, A. K.; Gorzelany, J.; de Souza, M. Phage display-derived peptides as therapeutic alternatives to antibodies. *Drug Discovery Today* **2004**, *9*, 525–529.
(34) Byrne, M. F.; Corcoran, P. A.; Atherton, J. C.; Sheehan, K. M.; Murray, F. E.; Fitzgerald, D. J.; Murphy, J. F. Stimulation of adhesion molecule expression by *Helicobacter pylori* and increased neutrophil adhesion to human umbilical vein endothelial cells. *FEBS Lett.* **2002**, *532*, 411–414.
(35) William, C.; Schindler, R.; Frei, U.; Eckardt, K.-U. Increases in oxygen tension stimulate expression of ICAM-1 and VCAM-1 on human endothelial cells. *Am. J. Physiol.: Heart Circ. Physiol.* **1999**, *276*, 2044–2052.
(36) Bremerich, J.; Colet, J. M.; Giovenzana, G. B.; Aime, S.; Scheffler, K.; Laurent, S.; Bongartz, G.; Muller, R. N. Slow clearance gadolinium-based extracellular and intravascular contrast media for three-dimensional MR angiography. *J. Magn. Reson. Imaging* **2001**, *13*, 588–593.
(37) Vander Elst, L.; Raynal, I.; Port, M.; Tisnes, P.; Muller, R. N. In vitro relaxometric and luminescence characterization of P792 (Gadomelitol, Vistarem), an efficient and rapid clearance blood pool MRI contrast agent. *Eur. J. Inorg. Chem.* **2005**, *6*, 1142–1148.
(38) Laurent, S.; Vander Elst, L.; Muller, R. N. Comparative study of the physicochemical properties of six clinical low molecular weight gadolinium contrast agents. *Contrast Media Mol. Imaging* **2006**, *1*, 128–137.
(39) You, T. J.; Maxwell, D. S.; Kogan, T. P.; Chen, Q.; Li, J.; Kassir, J.; Holland, G. H.; Dixon, R. A. F. A 3D structure model of integrin $\alpha_4\beta_1$ complex: I. Construction of a homology model of β_1 and ligand binding analysis. *Biophys. J.* **2002**, *82*, 447–457.
(40) Irie, A.; Kamata, T.; Takada, Y. Multiple loop structures critical for ligand binding of the integrin α_4 subunit in the upper face of the

β-propeller model. *Proc. Natl. Acad. Sci. U.S.A.* **1997**, *94*, 7198–7203.
(41) Masumoto, A.; Hemler, M. E. Mutation of putative divalent cation sites in the α_4 subunit of the integrin VLA-4: distinct effects on adhesion to CS1/fibronectin, VCAM-1, and invasion. *J. Cell Biol.* **1993**, *123*, 245–253.
(42) Morikawa, H.; Hachiya, K.; Mizuhara, H.; Nishiguchi, S.; Shiomi, S.; Kuroki, T.; Kaneda, K. Sublobular veins as the main site of lymphocyte adhesion/transmigration and adhesion molecule expression in the porto-sinusoidal-hepatic venous system during concanavalin A-induced hepatitis in mice. *Hepatology* **2000**, *31*, 83–94.
(43) Wolf, D.; Hallmann, R.; Sass, G.; Sixt, M.; Kusters, S.; Fregien, B.; Trautwein, C.; Tiegs, G. TNF-α-induced expression of adhesion molecules in the liver is under the control of TNFR1—relevance for concanavalin A-induced hepatitis 1. *J. Immunol.* **2001**, *166*, 1300–1307.
(44) Jaruga, B.; Hong, F.; Kim, W.-H.; Gao, B. IFN-γ/STAT1 acts as a proinflammatory signal in T cell-mediated hepatitis via induction of multiple chemokines and adhesion molecules: a critical role of IRF-1. *Am. J. Physiol.: Gastrointest. Liver Physiol.* **2004**, *287*, G1044–G1052.
(45) Iiyama, K.; Hajra, L.; Li, M.; Iiyama, H.; DiChiara, M.; Medoff, B. D.; Cybulsky, M. I. Patterns of vascular cell adhesion molecule-1 and intercellular adhesion molecule-1 expression in rabbit and mouse atherosclerotic lesions and at sites predisposed to lesion formation. *Circ. Res.* **1999**, *85*, 199–207.
(46) Broisat, A.; Riou, L. M.; Ardisson, V.; Boturyn, D.; Dumy, P.; Fagret, D.; Ghezzi, C. Molecular imaging of vascular cell adhesion molecule-1 expression in experimental atherosclerotic plaques with radiolabelled B2702-p. *Eur. J. Nucl. Med. Mol. Imaging* **2007**, *34*, 830–840.
(47) Aime, S.; Botta, M.; Fedeli, F.; Gianolio, E.; Terreno, E.; Anelli, P. High-relaxivity contrast agents for magnetic resonance imaging based on multisite interactions between a beta-cyclodextrin oligomer and suitably functionalized Gd-III chelates. *Chem.—Eur. J.* **2001**, *7*, 5262–5269.
(48) Vander Elst, L.; Port, M.; Raynal, I.; Simonot, C.; Muller, R. N. Physicochemical characterization of P760, a new macromolecular contrast agent with high relaxivity. *Eur. J. Inorg. Chem.* **2003**, *13*, 2495–2501.
(49) Port, M.; Rousseaux, O.; Muller, R. N.; Burtea, C. Compounds for the Diagnosis of Apoptosis. European Patent WO 2008/125420 (A2), 2008.